JOURNAL OF MATERIALS SCIENCE 10 (1975) 1194–1227

Review
Flow and fracture in amorphous alloys

CARLOS A. PAMPILLO
ALUAR (Aluminio Argentino), Puerto Madryn, Chubut, Argentina

This paper reviews the flow and fracture properties of amorphous metals synthetized by fast quenching from the liquid state. The data are analysed in conjunction with recently proposed theoretical models.

1. Introduction

This paper reviews the plastic flow and fracture characteristics of amorphous metals prepared by quenching from the liquid state. Amorphous metals have been also synthesized by electro- or chemical deposition [1] and vapour deposition [2] but the mechanical properties of the solids so formed will not be included here.

The first amorphous metal produced from the liquid state was an alloy of Au and Si obtained by Klemens *et al.* [3] while investigating metastable solid solutions by fast quenching techniques. In the 12 years since that discovery, very many metallic alloy systems which are capable of forming amorphous solids have been found. A considerable amount of work has been accumulated during those years on the structure and thermodynamic, electronic and mechanical properties of amorphous metals. The results of this research effort have opened a new and important chapter in materials science. The recent announcement of developments in structural and other applications of these metallic solids [4, 5] indicates that they will very probably become an important chapter in technology as well. What were once called "Duwez's stupid alloys" [6] are proving to be something very different.

Part of the research work has recently been reviewed in considerable detail [6-8]. However, only in the last three years or so, strong interest started to develop in the elastic, plastic flow and fracture properties of amorphous metals. A substantial part of the work on these properties has not appeared in the earlier reviews. Therefore, this work attempts to close that gap somewhat.

2. Brief considerations concerning the structure and formation of metallic glasses

2.1. The atomic structure

Examination of amorphous metals by X-ray or electron diffraction shows the diffuse diffraction halos which may be taken as characteristic of amorphicity. However, this characteristic alone is not sufficient to characterize the atomic arrangements within the solid. In fact, the two limiting structural models proposed to describe such arrangements are able to explain the lack of a sharp diffraction pattern [9]. These are the microcrystalline [10] and the continuous random network models [11] also proposed to describe the atomic structure of the liquid state. The structure proposed in the microcrystalline model consists of an aggregate of small imperfect crystallites. The well-known widening of the X-ray diffraction peaks due to small crystallite size will eventually lead, below a certain size (5 to 10 atomic diameters) to a diffuse diffraction halo. The continuous random network, on the other hand, postulates a structure where there are no discontinuities in atomic structure such as one would expect from the microcrystalline model, where a crystalline phase and an intercrystallite phase must necessarily co-exist.

Evidence from crystallization, which occurs by nucleation and growth with a dendritic morphology [9] and from heat capacity [12, 13] and rheological [12] measurements, which show the existence of a glass-metastable liquid transition, suggests that these solids have a continuous structure and, therefore, only one phase. Moreover, detailed X-ray diffraction studies show that there is a good agreement between experimental

data and the predictions of a continuous random model [15].

2.2. Metallic glass compositions

Many of the metallic systems reported lately, which are susceptible to form glasses when quenched from the liquid state, have been reviewed by Giessen and Wagner [7] and by Anantharaman and Suryanarayana [16]. These alloys are generally formed by a mixture of a noble or transition element and a high valence metalloid such as P, C or Si [7, 16, 17]. The composition of the glass-forming alloys are generally within a small composition range, around the 20 at. % metalloid content. This rather narrow composition range is explained by Polk's structural model [18] where the metalloid atoms are included in the larger holes left within a "relaxed"* [19] dense random packing of the metal atoms. An exception to this is found in the Cu–Zr glass-forming alloys, recently reported by Ray *et al.* [22] which do not contain any metalloids and are around the 50:50 at. % composition.

The tendency to form glasses in these systems has been discussed recently by Turnbull [17] and by Giessen and Wagner [7]. Some important factors which may contribute to stabilize the amorphous phase are:

(1) The higher complexity of the atomic structure of the stable or metastable crystalline phases of the alloys. This makes difficult the atomic rearrangements required for crystallization;

(2) A strong repulsive interaction probably exists between the cores of the noble or transition metals. This would lead to a higher glass transition temperature [21];

(3) A size difference between the atomic species in the alloy [23, 24] which may lead to a greater efficiency in filling space and hence to a decrease in the energy of the amorphous phase;

(4) A greater attractive interaction between the metal and metalloid atoms relative to the metal–metal or metalloid–metalloid interactions. This leads to a composition short range ordering which should stabilize the amorphous state as suggested by Polk [18].

In general terms, it is possible to increase the susceptibility to glass formation by introducing factors which lower the thermodynamic melting point (T_m), delay crystallization (C) or increase the glass transition temperature (T_g). This is shown schematically in the temperature-time-transformation diagram in Fig. 1. The arrows indicate changes leading to greater glass forming susceptibility or stability of the amorphous phase.

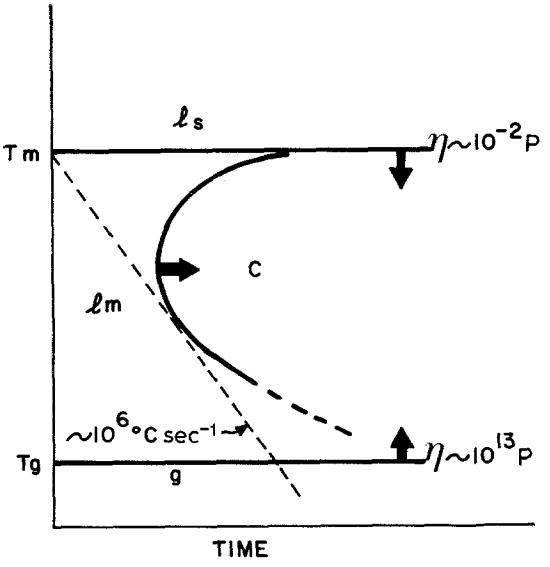

Figure 1 Temperature-time-transformation diagram for crystallization. Schematic. T_m is the thermodynamic melting temperature; T_g the glass transition temperature; c, crystalline phase; g, glassy or amorphous phase; l_s stable liquid and l_m metastable liquid.

2.3. The glass–liquid transition

Above the glass transition temperature the viscosity of the liquid is generally small, and the atomic relaxation times are small fractions of a second. If crystallization does not occur, the liquid can be brought to internal equilibrium rather rapidly. As the temperature is lowered, the relaxation times increase and close to T_g they become of the order of the experimental times (a few seconds). With decreasing temperature to a few degrees below T_g, the relaxation times very rapidly increase to exceedingly large values. The atomic arrangements become "frozen" and the alloy solidifies with the structure of the metastable liquid at a temperature close to T_g. The metastable liquid–glass transition and the ensuing solidification is due to this very fast, but continuous, change in the relaxation times which occurs around T_g.

The contribution of the atomic rearrangements and vibrations to the specific heat, C_p, and

*By "relaxed" we mean a "more loosely random packed structure" [19] (see also [17]).

volume, v, which above T_g are characteristic of the liquid, disappear in a continuous way within a small temperature range around T_g. Below T_g, C_p and v attain values which are characteristic of the solid. In the metallic glasses these values are above, but very close to, those of the stable crystalline phase [12, 25-27] as shown schematically in Fig. 2.

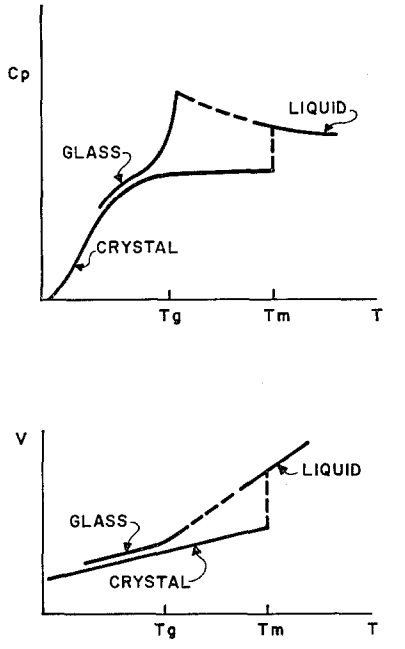

Figure 2 Specific heat [12] and specific volume (schematic) as a function of temperature.

Some characteristics of the glass–liquid transition have been explained by the free volume theory of Cohen and Turnbull [28]. The relatively high densities found in metallic glasses (98% of the crystalline density) are explained by the binary dense random packing model proposed by Polk [18].

With increasing temperature, the trends discussed above are reversed. However, contrary to some more stable oxide and polymeric glasses, at the heating rates commonly used in a microcalorimeter (20°C min^{-1}), all metallic glasses crystallize before reaching the stable liquid at T_m. Crystallization occurs at a temperature T_c a few degrees above T_g [12]. In some cases, crystallization occurs before the glass transition temperature is reached [14]. The difference $T_c - T_g$ has been proposed as a measure of the relative stability of the metallic glass [12]. At temperatures below T_g, crystallization occurs after much longer annealing times.

2.4. Quenching techniques

In order to continuously solidify the metallic liquid, bypassing the "crystalline boundary" as shown schematically by the dotted line in Fig. 1, high quenching rates, of the order of 10^6°C sec^{-1} are required. High quenching rates have been obtained by striking small amounts of the liquid alloy with or on to a substrate which is an efficient extractor of heat. The several techniques developed have been reviewed by Duwez [6] and more recently by Willens and Giessen [8] and Giessen and Wagner [7].

With the exception of the quench-rolling (QR) technique of Chen and Miller [29] and of Babić *et al.* [30] and the rotating cup (RC) technique of Pond and Maddin [31] all other techniques produce metallic glass samples which are small or irregular in thickness and are therefore not suitable for mechanical studies. The two mentioned techniques have only recently been applied to synthetize amorphous metals and, therefore, the study of the mechanical properties of these solids was delayed for many years.

In the QR technique, the molten alloy is allowed to drop from an orifice at the bottom of a crucible into the closed gap of a pair of fast rotating rollers. If the liquid metal falls exactly between the two rollers, it is squeezed and rapidly quenched from both sides. In the RC technique, the liquid metal is ejected from an orifice placed on the side of a crucible. The liquid stream is then cooled when it hits a metallic cup rotating around the crucible.

In both techniques the final product is a strip generally 0.003 cm thick, 0.1 cm wide and several metres long. The quenching rates have been estimated to be of the order of 10^6°C sec^{-1}.

The flow and fracture properties reviewed below have been studied on glass specimens prepared by either of the two techniques mentioned above or modified versions of these techniques. Except for a few cases, all these glasses display a glass–liquid transition before crystallizing, as evidenced by microcalorimetry.

3. Ductility

A general reaction is to associate glassiness with brittleness. The common experience of the shattering of silicate glasses (window glass, pyrex, etc.) is probably responsible for this

association. However, organic polymeric glasses can be considered as ductile glasses. Both inorganic oxides and organic polymeric glasses are covalently bonded. Polymeric glasses also have much weaker van der Waals or hydrogen bonds which hold together the covalently bonded chains. This mixture of bonding within the same solid is, in part, responsible for the higher ductility in these glasses as compared with the totally covalently bonded inorganic glasses, since they allow enough sliding between polymer chains to provide a means of dissipating elastic energy without cracking.

The long covalently bonded chains, however, establish strong links that keep the structure together. On the other hand, the strong and localized bonding in inorganic oxide glass leads to the brittleness typical in these glasses; there is almost no easy way to dissipate elastic energy without bond scissions and cracking, i.e. plastic flow is difficult in most typical conditions.

In metallic glasses, bonds between atoms are not as localized as in silicate glasses and one would expect that it is possible to dissipate elastic energy through plastic flow. However, the fact that generally metallic glasses contain substantial amounts of metalloidal elements means that to some extent, the atomic bonding existent in these glasses may have a covalent character.

Experimentally, are metallic glasses found to be ductile? The lack of precision in the word "ductility" prevents us from answering this question in an unambiguous way; as in "beauty" the meaning of the word lies more with the observer than with the object under observation.

If we hold ductility to be a measure of plastic strain before failure, whatever its distribution, then many metallic glasses could range with the most ductile organic polymeric glasses or crystalline metals: very high plastic strains occur before fracture. These plastic strains are highly localized, however. An illustration of the extent of localized plastic flow is shown in Fig. 3 which refers to a $Pd_{77.5}Cu_6Si_{16.5}$* glass rod deformed in compression at room temperature [32]. Intersecting slip bands showing plastic strains as great as $\gamma \approx 2$, appear at the free surface of the specimen. Within the resolution of a two stage plastic replica viewed with an electron microscope (~ 100 Å resolution) no other slip bands or lines are found between those visible with the optical microscope. The glass slips by shear in a few narrow zones; the rest of the solid remaining rigid. An entirely different type of concentrated flow is shown in the scanning electron micrograph in Fig. 4.† It was taken from a small region on the fracture surface of the same glass fractured in torsion. This area was probably the last to fail and did so in tension (the torque was applied by hand). The extremely large concentrated flow, which led to the internal "ductile rupture" of this portion of the specimen, probably occurred after some localized heating due to the deformation and fracture of the surrounding areas. These two cases show that although localized, very large amounts of plastic flow can occur without cracking. Regarding

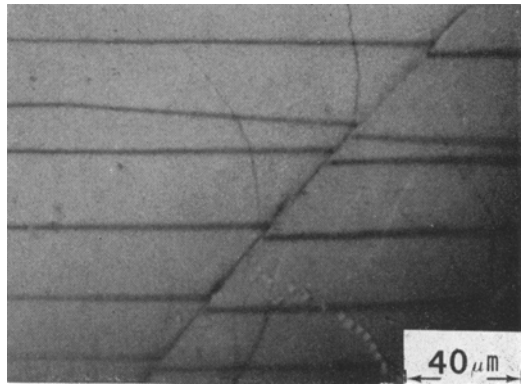

Figure 3 Shear bands in a bulk $Pd_{77.5}Cu_6Si_{16.5}$ glass. Optical micrograph (OM).

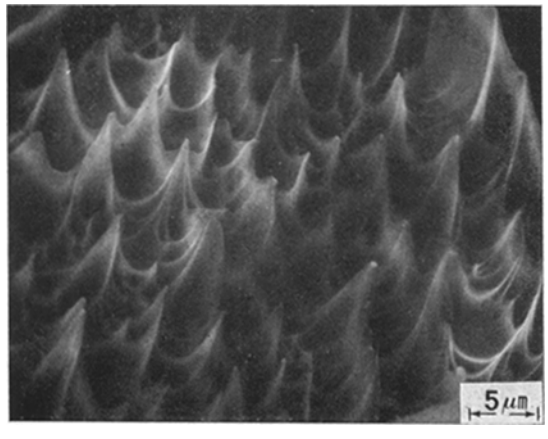

Figure 4 Region of the fracture surface of a $Pd_{77.5}Cu_6Si_{16.5}$ glass rod fractured in torsion (SEM).

*The subscripts denote the concentration of the element in at. %.
†Similar torsion fracture features have been observed by Leamy [33].

ductility, this puts metallic glasses higher in the hierarchy than inorganic oxide glasses.

However, plastic flow must be well distributed if the solid is to respond in a macroscopically ductile way. In uniaxial tension, for instance, the high localized plastic strain leads to a tensile elongation of only $\sim 0.5\%$ [34] on specimens 2.5 cm long. Plastic flow may become better distributed if the external geometrical constraint imposed on the glass specimen helps it to do so.

Large macroscopic plastic strains without cracking are found to be possible in rolling: a 0.15 cm diameter rod of $Pd_{77}Cu_{6.5}Si_{16.5}$ glass was rolled at room temperature to a 0.025 cm ribbon without showing any signs of cracking. Also, Fig. 5 shows a ribbon, 0.0025 cm thick, of a $Ni_{49}Fe_{29}P_{14}B_6Al_2$ glass, produced by a modified RC technique, bent over the edge of a razor blade [35]. No cracks are found on a cross-section polished normal to the bending axis. Plastic flow, although inhomogeneous, is spread over a greater volume of the solid, than in a tensile test, allowing greater macroscopic ductility. Similar results have been obtained with $Pd_{77}Cu_{16.5}Si_{6.5}$, $Pd_{77.5}Ni_6Si_{16.5}$, $Pd_{64}Ni_{16}P_{20}$, $Pt_{60}Ni_5P_{25}$ and $Ni_{75}P_{15}B_{10}$ glasses but not with a $Fe_{75}P_{16}C_9$ glass which showed cracking upon the same deformation. It was suggested that this brittleness is inherent to the Fe-base glasses [36].

These experiments qualitatively show that, in general, depending on composition, metallic glasses have inherent ductility. However, they deform plastically by highly concentrated shear flow which leads to a small macroscopic ductility. Only if, by external means, the inhomogeneous flow can be forced to occur on a larger volume of the solid, can one obtain with some metallic glasses macroscopic ductility which is comparable to that in polymeric glasses or crystalline metals.

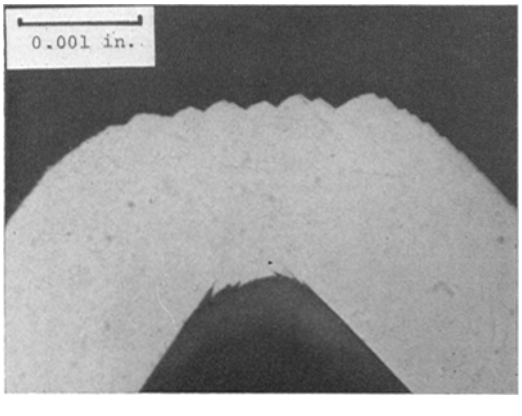

Figure 5 $Ni_{49}Fe_{29}P_{14}B_6Al_2$ glass ribbon bent over a razor blade [35] (OM).

4. The inhomogeneous plastic flow in metallic glasses

Strong inhomogeneous plastic flow, such as that shown in Fig. 3 has been observed in several metallic glasses namely $Pd_{80}Si_{20}$ [37], $Pd_{82}Si_{18}$, $Pd_{79.5}Au_4Si_{16.5}$ [34], $Pd_{83}Si_{17}$, $Pd_{78}Si_{22}$ [38], $Ni_{72}P_{18}B_7Al_3$, $Ni_{49}Fe_{29}P_{14}B_6Al_2$, $Fe_{76}P_{16}C_4Al_2Si_2$ [40], $Ni_{75}P_{15}B_{10}$, $Pt_{60}Ni_{15}P_{25}$, $Pd_{64}N_{16}P_{20}$, $Pd_{77.5}Ni_6Si_{16.5}$ [36] and $Cu_{50}Zr_{50}$ [41].

In the previous discussion, this mode of plastic flow has been pointed out as an important factor determining macroscopic ductility. From a phenomenological point of view, inhomogeneous plastic flow is due to a lack or exhaustion of the ability of a solid to strain-harden. In terms of the micromechanisms for plastic flow, the study of the dynamics of dislocation motion gives a plausible explanation for the small or negative strain hardening which leads, in some crystalline solids, to concentrated flow. The level of understanding of the micromechanisms of flow in amorphous solids is far from that reached in crystalline solids. It may, therefore, be difficult to establish with some degree of certainty the atomic mechanisms responsible for the inhomogeneous mode of plastic flow. However, some factors leading to localized flow have been pointed out and are reviewed here.

The lack of inherent strain hardening in a metallic glass was first demonstrated by Pampillo and Chen [32] by showing that many shear bands which had been initiated early in a compressive deformation experiment with a $Pd_{77}Cu_{6.5}Si_{16.5}$ glass, would remain active up to large macroscopic strains. The macroscopic strain was totally provided by the operation of a few slip bands crossing the specimen; within these bands plastic strain became highly concentrated.

Another way to demonstrate the inherent lack of work hardening in a metallic glass is provided in Fig. 6a and b [42]. A 0.0025 cm thick strip of $Pd_{83}Si_{17}$ glass, prepared by a modified RC technique, was bent sharply and the slip steps appearing on the tension side were recorded by a scanning electron micrograph (Fig. 6a). The specimen was then bent back, the same area located and the microphotograph in Fig. 6b was obtained. Parallel arrows in (a) and (b)

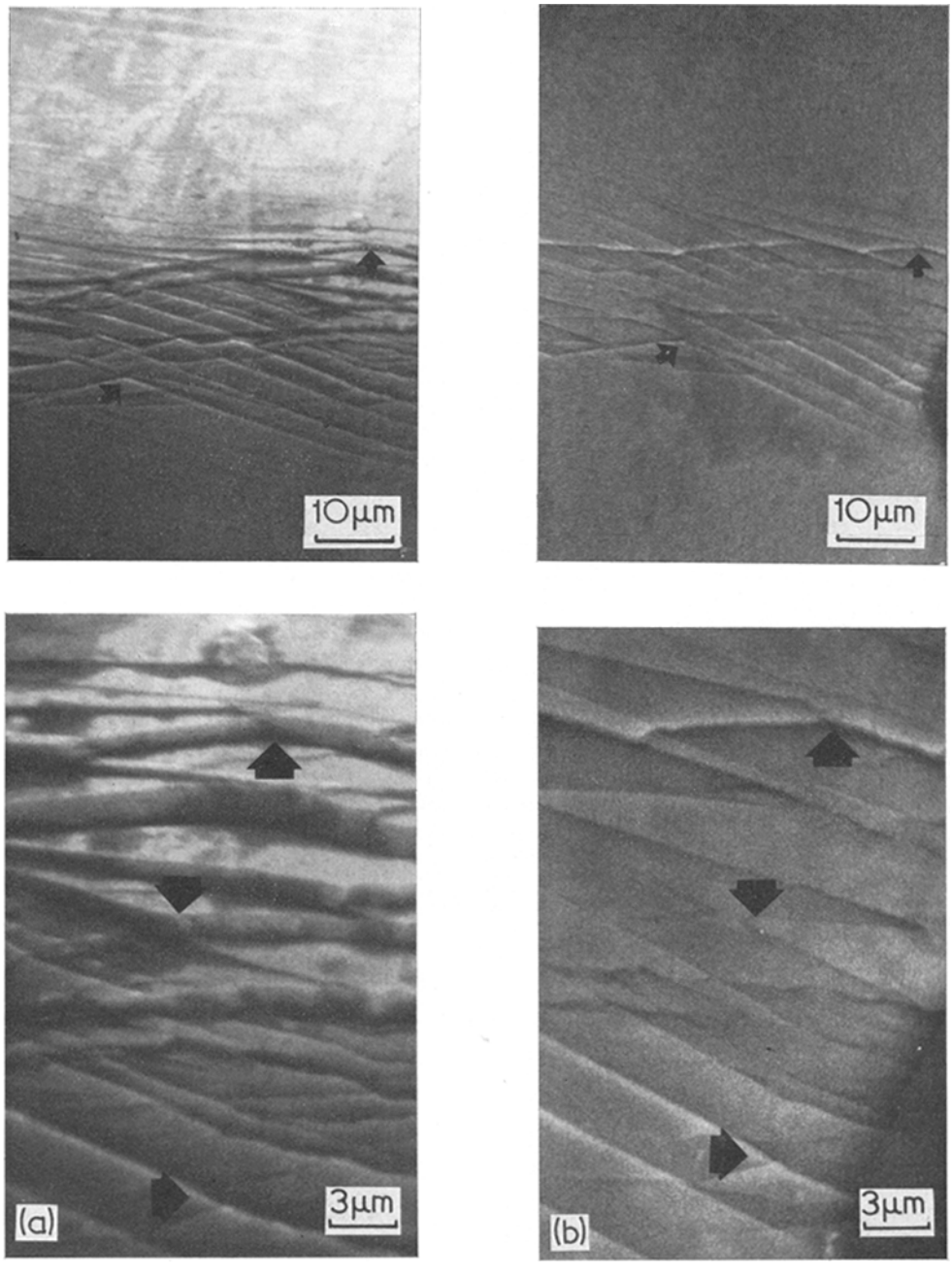

Figure 6 Reversibility of the operation of slip bands in $Pd_{83}Si_{17}$. (a) Slip bands formed by bending a ribbon of the glass. (b) reversal of slip displacement in slip bands by reversed bending [42] (SEM).

refer to the same spots on the specimen. As we can see, reversed shear deformation has occurred along the same slip bands that produced the initial deformation. No new slip bands have been nucleated. On careful examination, one finds that slip bands which were initially not too strong, almost disappear when the deformation is reversed. This experiment qualitatively shows that the flow stress within slip bands has become smaller than that outside them.

This behaviour is quite remarkable and clearly different from that experienced with crystalline metals where plastic flow can never be reversed along the same path on which it was initially produced and it seldom becomes as concentrated. The experiment also suggests that plastic flow produces a structure which facilitates further plastic flow.

Polk and Turnbull [43] suggested the possibility that, at temperatures below the glass transition temperature, plastic flow could destroy the compositional and/or structural short range order in the glass leading to concentration of plastic flow. Experimental support for this suggestion was provided by the author [44] who found that the slip bands on a deformed $Pd_{77}Cu_{6.5}Si_{16.5}$ glass could be preferentially etched demonstrating that a different chemical potential existed within shear bands. Shear bands which are revealed by preferentially etching a polished deformed glass specimen, are shown in Fig. 7 [44]. This etching sensitivity disappeared if the glass was heat-treated for 1 h at about 50°C below the glass transition temperature. No detectable changes occur in the undeformed glass by such a heat-treatment. Since at that temperature the driving force is to increase order, the annealing experiment indirectly supports the idea that the change in structure due to deformation is one producing a decrease in order. The etching sensitivity of slip bands was later confirmed in several other metallic glasses [36].

As part of the disorder created by plastic flow, the destruction of compositional order means that an increase in the number of metal–metal bonds across the slipped surface is created, at the expense of (very probably stronger) metal–metalloid bonds. This should lead to a decrease in the flow stress within shear bands giving rise to an easy path for further deformation. The structural disorder created within slip bands could be in the form of an increase in the average atomic volume [43] or dilation [45] associated with plastic flow. The combination of a destruction of compositional order and dilation within bands may lead to a critical or limiting structure within the band that allows deformation at a stress lower than that required to deform the virgin matrix. Beyond the attainment of this limiting structure, the flow stress within the band probably also reaches a constant limit. It is easy to see that the destruction of compositional order by shear flow has a limit. This limit is a structure with a random distribution of atomic species which may be reached after sufficient strain within a slip band.

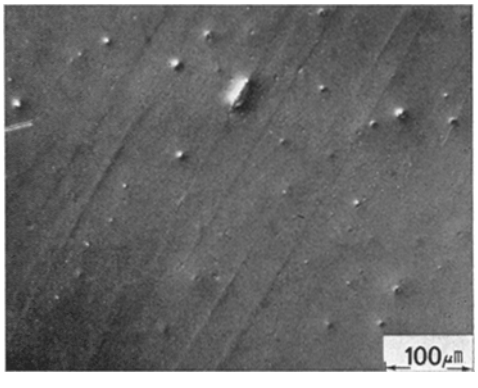

Figure 7 Shear bands in $Pd_{77.5}Cu_6Si_{16.5}$ glass appearing by preferential etching of a polished deformed compression sample [44] (OM).

The situation is analogous to that occurring in granular materials, e.g. dense sand, where it has been shown that shear failure takes place with "dilation" of the aggregate. This change in volume occurs within the narrow slip band along which shear deformation and final failure occurs; the rest of the sample remains essentially rigid [46, 47]. The material within the slip band acquires a so called "critical state"; beyond this state, deformation occurs at constant volume and stress [46, 47].

Leamy *et al.* [34], on the other hand, have suggested that the concentration of plastic flow is due to the heating effect produced by plastic deformation, i.e. by "adiabatic shear". The increase in temperature within the deforming band is considered to be high enough to produce softening of the glass and promote further slip. However, let us consider a shear band of thickness $2h$ operating under a stress τ and deforming at a rate $\dot{\gamma}$ (within the band) [48]. The maximum temperature rise will occur at the middle of the band. If the deformation event occurs in a time $t < h^2/4k$, where k is the thermal diffusivity, then the heating effect at the middle of the band will be almost adiabatic and the temperature rise there will roughly be $\Delta T \approx (\tau\dot{\gamma}/\rho C_p)t \approx \tau\dot{\gamma}h^2/4\rho C_p k$, where ρ is the density and C_p the specific heat (we have considered that all the plastic work is converted into heat). The worst case will be that in which the specimen deforms by slip within only one band. The plastic strain rate $\dot{\gamma}$ within the band is then roughly $\dot{\gamma} \approx \dot{l}/2h$, where $\dot{l}$ is the

machine cross-head speed. The temperature rise is then $\Delta T \approx \tau \dot{l} h / 8K$, where $K = \rho C_p k$ is the thermal conductivity. With $\tau \approx 150$ kg mm^{-2}, $K = 0.143\ 10^7$ erg cm^{-1} sec^{-1} K^{-1} [49] (this value is for glassy $Pd_{82}Si_{18}$ at room temperature) we find $\Delta T \approx 40 \dot{l} h$ where $\dot{l}$ is in cm sec^{-1} and h in cm. This shows that for a band, say, 10^{-2} cm thick the temperature rise will be 40°C if $\dot{l} \approx 10^2$ cm sec^{-1}. In most tests, the temperature rise within the shear bands in glassy metals will, therefore, be quite small (typically $\dot{l} \approx 10^{-2}$ cm sec^{-1}; $h \approx 10^{-4}$ cm). Higher temperature rises may be expected at very low temperature where C_p becomes small [50].

Finally, we should point out the fact that some polymeric glasses, which are known to have a continuous random structure also deform by extremely inhomogeneous shear [51]. This shows that inhomogeneous shear slip cannot be taken as evidence of microcrystallinity, as suggested recently [4].

5. Microscopic modes of fracture in metallic glasses

The terms "ductile" or "brittle" are also used to qualify the microtopography formed on the fracture surfaces of solids. Cleavage, although it may occur on fracture of a tensile bar after extensive plastic deformation (macroscopic ductility), is referred to as a brittle microscopic mode. Dimpled rupture, on the other hand, may be found on the fracture surfaces of tensile specimens that failed before general yielding (macroscopic brittleness), but is referred to as a ductile microscopic mode of failure. The classification of these modes into "brittle" or "ductile" stems from the energy required for the final crack propagation producing the failure rather than from the amount of prior plastic flow.

Although no measurements of the energy for crack propagation in metallic glasses have been reported,* a separation between ductile or brittle microscopic modes of failure may be qualitatively attempted just from the appearance of the topographical features on fracture surfaces and under what conditions they appear. The different microscopic modes of fracture may be a result of different temperatures, alloy compositions or heat-treatments. In general, as we shall see, these different microscopic modes of fracture relate to different macroscopic behaviour, namely fracture stress, ductility in bending, angle between the fracture surface and the tensile stress and fragmentation. The observed microscopic modes will be reviewed here and will be considered also in the next section in connection with the flow and fracture stress. We first discuss the microscopic mode of fracture which, in the author's experience, is most common in metallic glasses prepared by the QR or RC technique, and then review other fracture modes that have also been reported.

5.1. The "pseudo-cleavage" microscopic mode

Leamy *et al.* [34] were the first to report on the microscopic features found on the tensile fracture surfaces of some Pd–Si-based specimens. The specimens were thin Pd–Si-based glass strips prepared by the quench-rolling technique. The fracture topography found was described as a "vein" pattern formed by protrusions produced by local necking. By comparing the features on matching fracture surfaces, they concluded that failure happened after a shear displacement had occurred along a plane whose normal formed an angle of 45° with the tensile axis and the thickness vector. Matching fracture surfaces of a $Pd_{77.5}Cu_6Si_{16.5}$ rod specimen broken in tension are shown in Fig. 8 [52]. The initial shear displacement is shown between the edge of the specimen and the arrows. The same letters refer to matching fracture features. The higher magnification SEM micrographs in Fig. 9a and b give a clear view of the "vein" pattern. Except for the ridges forming the veins the fracture surface is flat and on close examination, the surface in Fig. 9b is found to be very smooth. Leamy *et al.* [34] suggested that this type of fracture is due to the adiabatic heating created by plastic flow. This, in turn, leads to the localized deformation and eventually the specimen fails and leaves the vein pattern.

A somewhat similar view although with a different mechanism is that of Spaepen and Turnbull [53]. The fracture pattern formed is considered to be the result of the breaking of a fluid layer between two solid surfaces. The fluid layer (the slip band) is formed because of the increased "free volume" created by the hydrostatic tension existent at the head of a growing band. This lowers the viscosity within that region down to values typical of a fluid. In both models an important role is played by the rapid

*Measurements of the fracture toughness of glassy alloys have been performed. These are discussed in Addendum A.

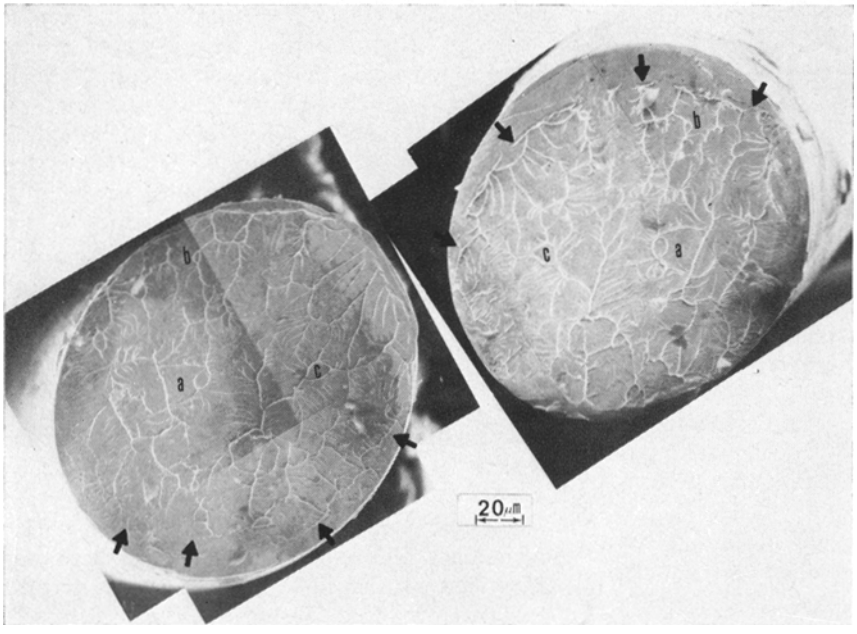

Figure 8 Matching fracture surfaces in a $Pd_{77.5}Cu_6Si_{16.5}$ glass specimen that failed in tension [53]. The initial shear displacement is shown between the edge of the specimen and the arrows. The same letters refer to matching fracture features. (SEM).

softening of the solid which occurs close to the glass–liquid transition.

A different viewpoint was presented by the author and Reimschuessel [52]. It was proposed that the concentrated shear deformation prior to failure defined a weaker "pseudo-cleavage" plane on which nucleation and propagation of cracks would occur with greatest ease. The weakening of the sheared plane was thought to occur as a result of the structural changes occurring within the band and already discussed in the previous section. The main ridges or veins are formed where pseudo-cleavage cracks, nucleated at different sites on the

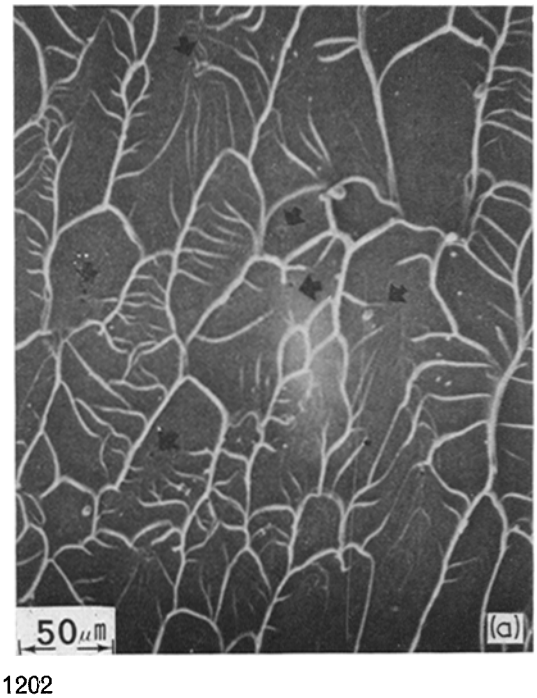

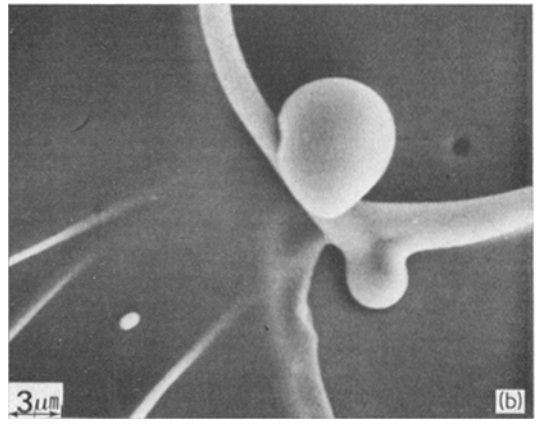

Figure 9 (a) "Vein pattern" on the fracture surface of Fig. 8. (b) Higher magnification showing the smothness of the main fracture surface. It also shows that the veins are ridges and not steps [52] (SEM).

sheared plane, coalesce. Necking coalescence, as opposed to "cracking through", was thought to be the result of the change in the stress state at the crack tip and the poor heat extraction conditions which occurs when two advancing pseudo-cleavage cracks are close to collision. The heating effect at the point of coalescence becomes more evident (because of least heat extraction conditions) at triple vein points where filaments with rounded tips are formed Fig. 9b, very probably by viscous flow.

The main vein is sometimes connected to a series of fingers or tributary veins which point to the crack nucleation site as shown in Fig. 10 [52]. The formation of these tributary "veins" or fingers is thought to be due to an inherent instability of the crack front probably because of the same factors leading to coalescence by necking considered above [52]. However, the resemblance of the tributary veins or fingers (Fig. 10) and the features which are formed when two glass slides which are held together by a viscous medium, are slowly separated (a to f)

Figure 10 Fingers or tributary veins pointing to a crack nucleation site. The fracture surface belongs to a $Ni_{49}Fe_{29}P_{14}B_6Al_2$ glass. The nucleation site, (arrow) is probably a hole left by an impurity particle [40] (SEM).

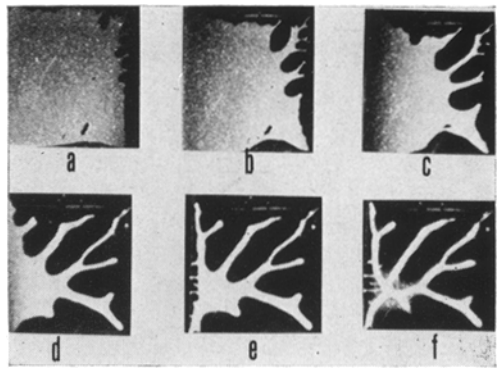

Figure 11 Simulated "crack" propagation by opening up two glass slides held together by grease. It illustrates the formation of tributary veins. The instability of the crack front producing the fingers is the Taylor instability [52].

Fig. 11, has been pointed out [52, 53]. The features formed in this case are due to the Taylor instability [54] which occurs at the moving boundary between two immiscible fluids in this case air and the viscous medium, vaseline. The intriguing question is whether the features in Fig. 10 could be due to the same Taylor instability, but occurring in the solid state.* This resemblance has also been considered as evidence of the formation of a fluid layer [53]. The fluid layer is thought to be nucleated at stress concentrations where the hydrostatic tension is high enough to induce free volume required for fluidization. The fluid region is considered to grow along the maximum shear stress plane and fails by cavitation after it has covered the whole cross-section of the specimen [53].

However, one does not understand why cavitation does not occur just after the fluid layer has been nucleated at a stress concentration, where the normal stress is much larger than when the fluid layer has developed completely across the whole specimen. This does not apply to the pseudo-cleavage model because failure initiates, at for instance, hard undeformable impurity particles (see below) after a certain amount of plastic strain required for void nucleation.

Cracks on the sheared plane are probably nucleated at impurity hard particles by interphase decohesion or void formation, due to the large plastic strain in the glassy matrix surround-

*This is quite possible since the only difference is that the "effective viscosity" is non-Newtonian.

ing the particle. "Pseudo-cleavage" propagates from the nucleation site until it meets other growing cracks, defining a pseudo-cleavage zone surrounded by a main vein. In Fig. 9a we can see several crack nucleating sites (arrows). These show up as small holes and one sometimes finds, nearby, particles which appear to have been pulled out from the solid, leaving the cavities. Qualitative microprobe analysis showed that generally the particles had compositions which agreed with that of the matrix; they could, therefore, be small crystallized portions of the glass. Preparation of the alloy, quenching techniques and glass stability are all influential factors, therefore.

Although we have referred to the pseudo-cleavage mode as if it were intrinsic to certain glassy metals, it should be pointed out that its occurrence is strongly related to the way in which the specimen is deformed macroscopically. For instance, Fig. 12 shows the fracture surface of a $Ni_{49}Fe_{29}P_{14}B_6Al_2$ specimen that failed after repeated sharp bending. When fractured in tension this glass fails by the pseudo-cleavage mode [40]. The absence of the vein pattern in Fig. 12 indicates that in order to produce failure by the pseudo-cleavage mode the external constraint must allow or promote the formation of a well defined shear slip surface across the specimen. This behaviour is different from that shown by crystalline metals where the microscopic mode of failure (cleavage, dimpled rupture, etc.) does not change whether the specimen is deformed in tension or bending.

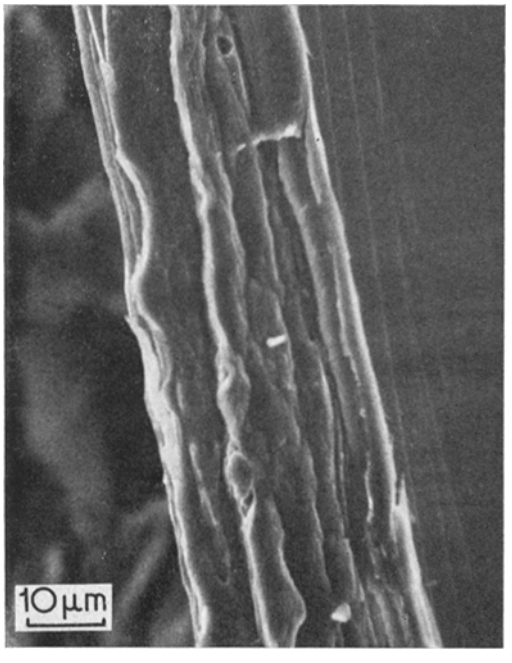

Figure 12 Fracture surface produced on a $Ni_{49}Fe_{29}P_{14}B_6Al_2$ glass ribbon by repeated bending (SEM).

Finally, Davis and Kavesh [55] have reported on tensile fracture surfaces of a $Pd_{77.5}Cu_6Si_{16.5}$ glass deformed under high hydrostatic pressure (6.9 kbar $\approx 10^5$ psi). Fig. 13, from their work, shows the tensile fracture surface produced at atmospheric pressure, at a, and at 6.9 kbar at b. At high pressure, the shear offset produced by slip before fracture is about three times larger. This is probably because hydrostatic pressure has delayed pseudo-cleavage crack propagation from crack nucleation sources within shear bands.*

At high pressure (Fig. 13b) cracking seems to be initiated peripherally rather than within the band as occurs at atmospheric pressure [55]. This is probably because the pressure fluid is able to aid crack opening only at the surface of the specimen, inducing a preference for peripheral cracks to run before those nucleated within the band.

The pseudo-cleavage microscopic fracture mode has been found on the fracture surfaces of $Pd_{82}Si_{18}$, $Pd_{79.5}Au_4Si_{16.5}$, $Pd_{77.5}Cu_6Si_{16.5}$ [34, 52], $Ni_{72}P_{18}B_7Al_3$, $Ni_{49}Fe_{29}P_{14}B_6Al_2$, $Fe_{76}P_{16}C_4Al_2Si_2$ [40] and $Cu_{50}Zr_{50}$ [41] glasses. As we shall see, in some glasses where this mode was not found at room temperature, it appeared at some higher temperature.

5.2. Other microscopic fracture modes

The pseudo-cleavage microscopic mode discussed above is suppressed, giving way to less ductile microscopic modes, as a result of changes in composition, temperature or heat-treatments. It has been reported (Pampillo and Polk, [40]) that, at room temperature, an $Fe_{76}P_{16}C_4Al_3B_1$ glass broken in tension does not show the pseudo-cleavage mode of failure which prevails in many other metallic glasses. The same is true for other Fe-based glasses such as $Fe_{77}P_{16}C_3Al_3B_1$, $Fe_{37}Ni_{37}P_{14}B_6Al_3Si_3$ and $Fe_{38.5}Ni_{38.5}P_{14}B_3Al_3Si_3$ [57].

An investigation over the temperature range 76 to 473 K was performed on the $Fe_{76}P_{16}C_4Al_3B_1$ glass [40]. The glass specimen strips were pre-

*Crack nucleation at hard particles does not seem to be affected by hydrostatic pressure [56].

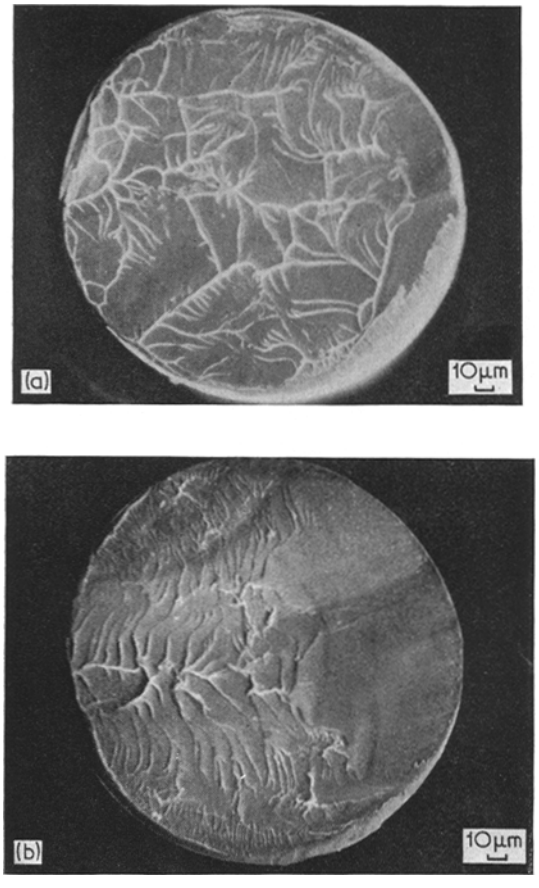

Figure 13 (a) Tensile fracture surface of $Pd_{77.5}Cu_6Si_{16.5}$ broken at 1 atm, and (b) broken at 6.9 kbar [55].

pared by a modified RC technique. At temperatures above room temperature, fracture took place only by the pseudo-cleavage microscopic mode already discussed, occurring along surfaces forming an angle of 45° with the tensile axis and the thickness vector.

Between room temperature and 200 K mixed fracture modes were found, including the pseudo-cleavage as shown in Fig. 14a at B and the shear displacement at A. Fracture seems to be also initiated by shear deformation along a plane at 45° to the tensile axis, A and B, but the final fracture occurs along a surface roughly normal to that axis. On this area, C, one finds, in some cases, features similar to a very fine and shallow dimpled rupture (Fig. 14b), typically found on low energy fracture surfaces, of high crystalline alloys [58].

Another change in the microscopic fracture mode is found at about 125 K for $Fe_{76}P_{16}C_4Al_3B_1$, and about 200 K for $Ni_{37}Fe_{37}P_{14}B_6Al_3Si_3$. Below this temperature, the initial shear deformation, which seems to trigger fracture at higher temperatures, disappears and the fracture surface appears flat with little or no traces of plastic flow (Fig. 15). As we shall see in the next section,

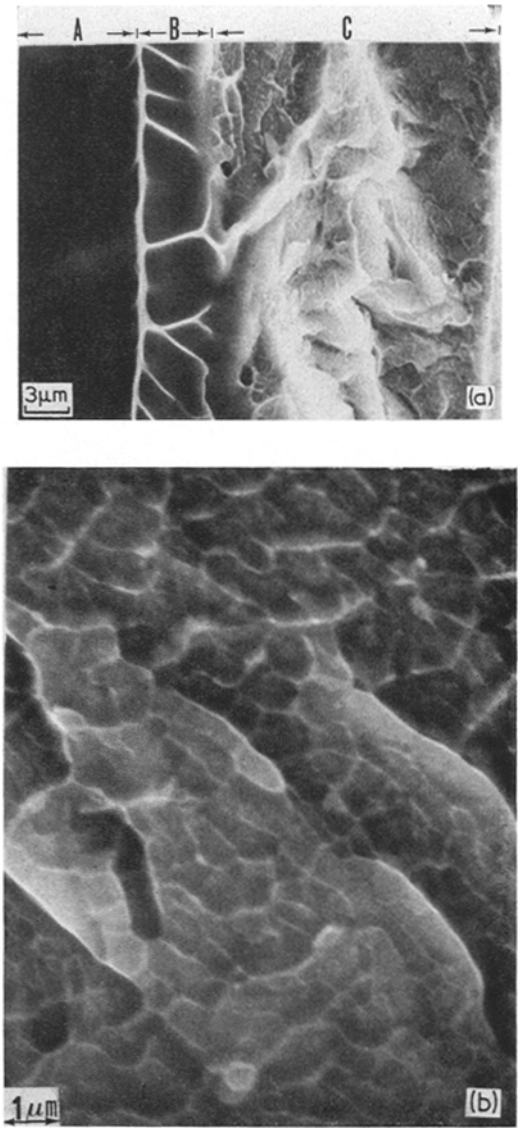

Figure 14 (a) Mixed fracture modes in $Fe_{76}P_{16}C_4Al_3B_1$ fractured in tension at room temperature. Region A is the shear displacement and B the vein pattern, of the pseudo-cleavage mode, occurring on a surface at an angle of 45° to the tensile axis. Region C is on a surface normal to the tensile axis [40] (SEM). (b) Microscopic features found on the fracture areas normal to the tensile axis. [40] (SEM).

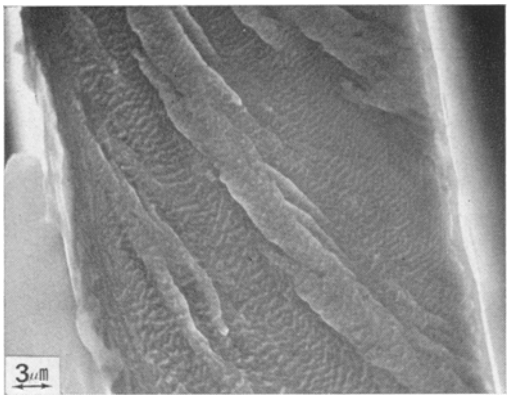

Figure 15 Fracture surface of $Ni_{37}Fe_{37}P_{14}B_6Al_3Si_3$ that failed at 190 K [57].

these changes are accompanied by changes in the fracture stress-temperature behaviour.

The change in fracture mode which occurs somewhat above room temperature in the $Fe_{76}P_{16}C_4Al_3B_1$ also correlates with the occurrence of fragmentation of the specimens upon failure [39]. It is found that at room temperature and at temperatures below this one, the Fe-base specimens shatter into several minute fragments. Above room temperatures, where the pseudo-cleavage fracture mode prevails, fragmentation does not occur but specimens are found with their fracture tips sharply curled up, suggesting that fragmentation in these specimens occurs by flexural waves, which are favoured by the low flexural rigidity of the thin specimens (25 μm thick) and probably not by tension waves (spalling).

Fragmentation does not occur in a $Ni_{49}Fe_{29}P_{14}B_6Al_2$ glass even at 76 K. This glass fractures by the pseudo-cleavage mode at all temperatures (76 to 500 K) [40]. It could be said then, that fragmentation occurs whenever the pseudo-cleavage microscopic fracture mode is absent, suggesting that the phenomenon is probably related to the energy for crack propagation in the metallic glasses.

It would be very useful if measurements of the energy for crack propagation in the different metallic glasses and at different temperatures were available to correlate them with the tensile fracture modes which appear at different temperatures. One expects to find the higher crack propagation energies whenever the pseudo-cleavage mode prevails.

A final observation which relates to fracture is that on Pd–Si glasses. Masumoto and Maddin [37] reported that, on optical examination, tensile fracture surfaces of $Pd_{80}Si_{20}$ appear normal to the tensile axis and show a fracture surface topography which resembles that of oxide glasses, i.e. having a "mirror like", "misty" and "hackle pattern" zones. These observations are at variance with scanning electron microscope observations of the tensile fracture surfaces of Pd–Si glasses ranging from 17 to 22 at. % Si [38]. In this case, fracture surfaces were found to lie at 45° to the tensile axis and the thickness vector.

However, the vein pattern typical of this failure mode (shear) is generally absent. Fracture surfaces appeared to be formed by shearing across the whole specimen without the final "pseudo-cleavage" cracking which leads to the vein pattern. This is seen in Fig. 16 which belongs to a $Pd_{82}Si_{18}$ glass. Two large "shear dimples" appear on the fracture surface. They were probably nucleated at impurity particles or voids. Except for these dimples, the fracture surfaces are flat and lacking any topographical features. With a few exceptions, where the vein pattern appeared on portions of a specimen, the same was found in the other glasses within the composition range investigated.

It is difficult to understand why this glass behaves rather differently. One factor that may be involved here is the density of crack nuclei within the glass. This factor will be related to the cleanliness of the glass, i.e. the amount of foreign particles or voids introduced during preparation, and possible crystallized particles which will be probably much harder than the matrix glass. If these particles are absent,

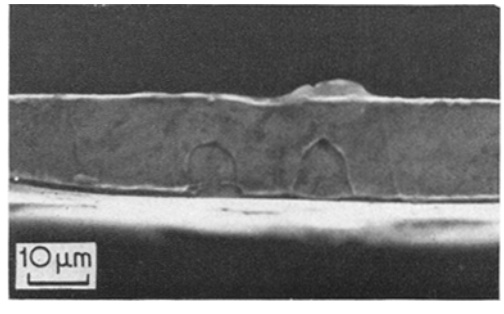

Figure 16 Fracture surface of a $Pd_{82}Si_{18}$ glass. Except for the two shear dimples, the surfaces lack any topographical features [38] (SEM).

simultaneous crack nucleation on different portions of the sheared surface will be difficult.

5.3. Stress corrosion experimental observations in a metallic glass

Stress corrosion cracking (SCC) in crystalline solids has been widely studied, but still the underlying atomic mechanisms controlling the nucleation and growth of SC cracks remains uncertain. Cracking by the combined effect of an applied stress and a corrosive environment occurs usually following grain boundaries [59], although single crystal experiments show that a polycrystalline aggregate is not a necessary condition for SCC [60]. In single crystals, SCC is associated with some crystallographic plane or anisotropic defect structure related to the crystal lattice.

There is no reason to believe that metallic glasses, although lacking a crystal lattice or grain boundaries, will not be susceptible to SCC. A simple stress corrosion experiment was performed with amorphous $Ni_{49}Fe_{29}P_{14}B_6Al_2$: tensile samples of the glass were loaded at a certain fraction of the fracture stress in air, immersed in a 3.5 N NaCl solution at 26°C and left in this condition until fracture occurred. Fig. 17a and b shows a specimen that failed after 117 h under an applied stress, 75% of the fracture stress in air. Fig. 17a shows a scanning electron micrograph of the fracture surface with the slow SCC growth at A and final fracture at B; (b) shows an optical micrograph of a polished cross-section (normal to the width vector) of the same specimen, with the fast fracture at B and SC cracks at A. The SC crack which lead to the final fracture is shown at C. One can see that the SC cracks grow normal to the applied tensile stress as is the case for crystalline metals [59, 60]. It is possible, however, that SC cracks have grown aided by slip bands forming at the tip of the SC cracks and breaking any passivating film that forms. Also, as we have seen in Section 4, slip bands seem to be anodic with respect to the rest of the undeformed matrix; one may, therefore, expect that slip bands may provide preferential corrosion paths.

A high magnification micrograph of the area selected in Fig. 17 is shown in Fig. 18. Fast fracture has occurred by the pseudo-cleavage fracture mode on a plane which is at an angle of about 60° to the tensile axis, see Fig. 17a (this departure from the 45° angle is probably due to the notch effect of the SC crack). The shear slip

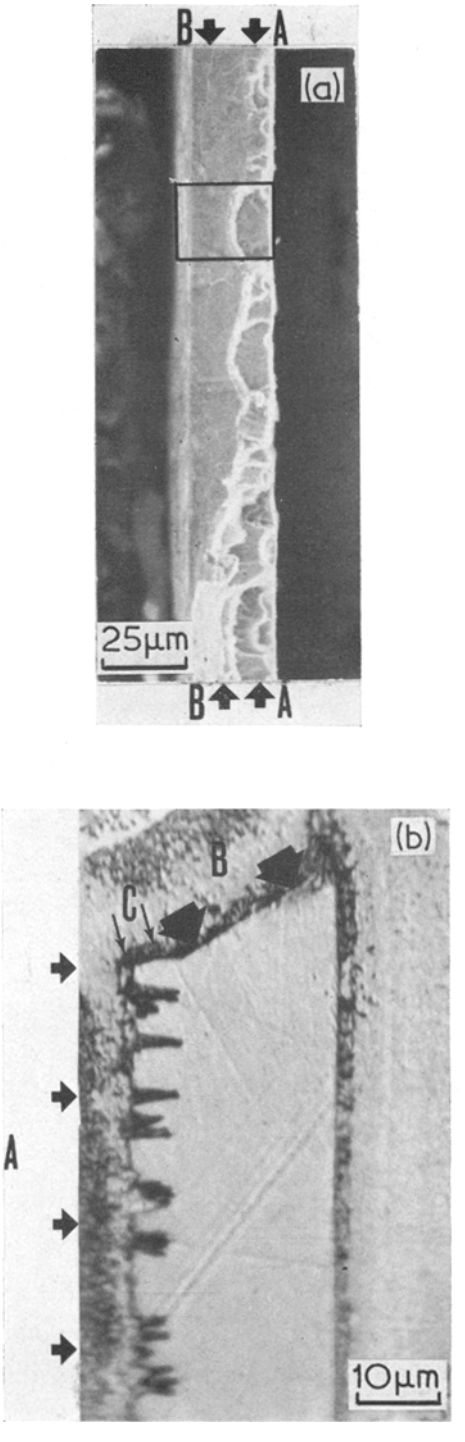

Figure 17 Stress Corrosion Cracking in $Ni_{49}Fe_{29}P_{14}Al_2$ glass. (a) is an SEM of the fracture surface, (b) is an OM of the polished cross-section (normal to the width vector) of the specimen. Arrows at A mark the stress corrosion crack growth area and at B the fast final failure.

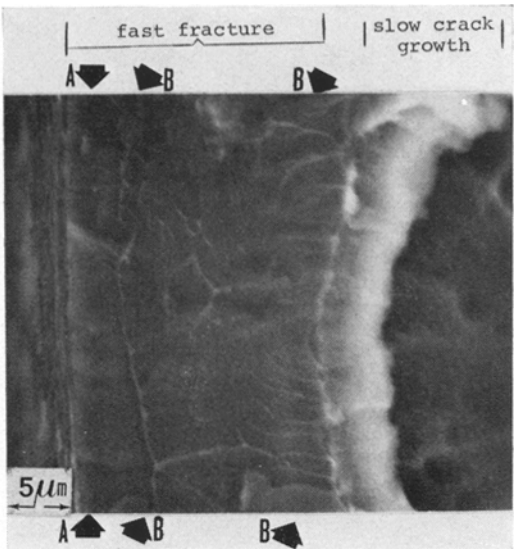

Figure 18 High magnification of the area selected in Fig. 17(a), showing the fast final failure area and slow stress corrosion crack growth area (SEM).

step is shown by arrows at A and the vein pattern by arrows at B. The growth of the SC crack has led to failure by prior shear yielding, just as it occurs when no cracks or notches are present, rather than by fracture normal to the tensile axis.*

Fig. 19 shows the slow SC crack growth area. The crack moved from right to left, leaving a smooth, almost featureless surface at the beginning of growth, and later a mottled area (left, Fig. 19). Qualitative microprobe analysis showed that the protrusions on the fracture surface were not corrosion products. The SC crack growth mechanism may have changed probably advancing, at the later stages, when the crack intensity factor is greater, by the formation of channels. These leave isolated islands which fail later on by a combination of tensile failure and disolution.

Nucleation of SC cracks seems to occur at an embrittled surface layer. There is evidence for this in Fig. 20 which shows the side of the specimen, far from the main fracture tip, and where SC cracks have not grown large enough. We can see a fine crack network similar to the "dry mud cracks" that form on inorganic oxide glasses [61]. SC cracks grow on the portions of these fine surface cracks which run normal to the tensile axis. As we approach the main fracture surface, upwards (Fig. 21), these cracks are

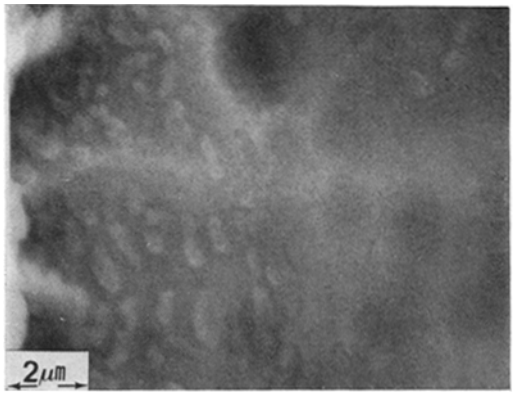

Figure 19 Slow stress corrosion crack growth area. The crack moved from right to left (SEM).

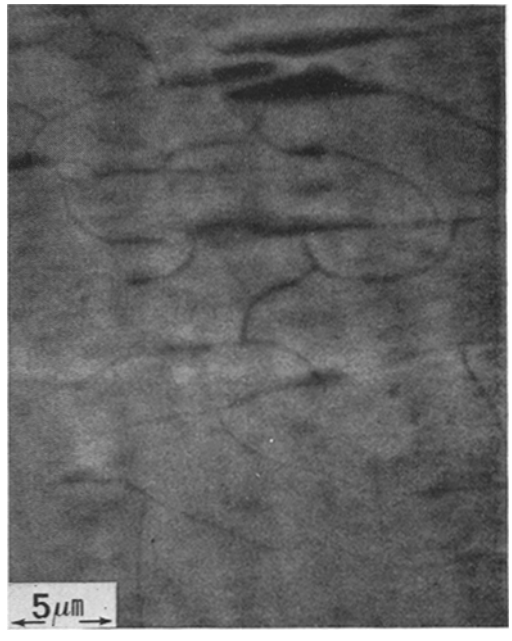

Figure 20 Side of the specimen far from the main fracture tip of the specimen, showing a fine surface "dry mud crack" pattern. Cracks grow on portions of the fine crack pattern which are normal to the tensile axis (SEM).

*This has been confirmed by Davis [62] in a $Pd_{77}Cu_{6.5}Si_{16.5}$ glass where cracks were introduced by fatigue (and were therefore quite sharp), but final failure still occurred by pseudo-cleavage and hence general yielding seems to occur always before fracture (at least in these two glasses). In the $Fe_{76}P_{16}C_4Al_2Si_2$ glass we have seen in Section 5.2 that below $\sim$ 200 K fracture occurs before general yielding.

found to have opened up and coalesce with each other as shown at the arrows. Dispersed on the areas between cracks one can see corrosion pits; these are also visible in Fig. 20. These two SCC nucleation mechanisms, i.e. cracking of a brittle surface layer and pitting, seem to compete with each other.

Although metallic glasses may not be exempt from stress corrosion, their single-phased structure with no grain boundaries makes us expect that the rate at which SCC occurs will be smaller than in high-strength crystalline alloys. Experiments to compare these two types of materials are necessary.

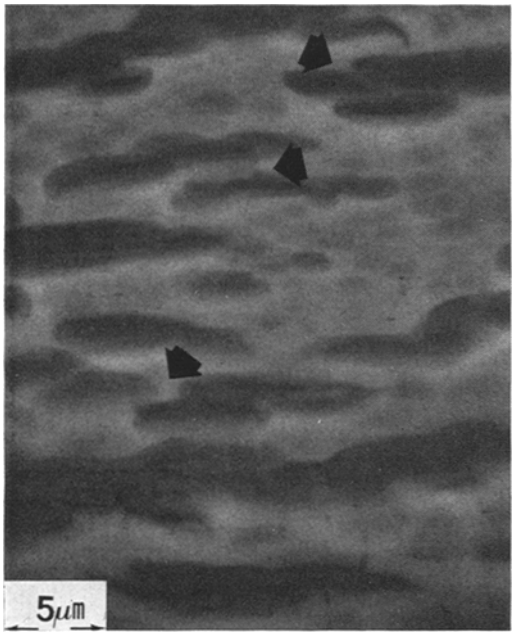

Figure 21 Area above that in Fig. 19, showing the opening up of stress corrosion cracks that nucleated on the fine surface cracks. The arrows point to places where coalescence of cracks is taking place (SEM).

6. The fracture and flow stress

With the advent of the RC quenching technique of Pond and Maddin [31] and the QR technique of Chen and Miller [29] and Babic *et al.* [30], mechanical testing of metallic glasses became easier and more reproducible. Several papers dealing with the tensile fracture and flow stresses of these solids have appeared in the last few years. The results of that work will be reviewed here. Whenever possible, the data will be related to the microscopic modes of fracture discussed in the previous section. We also discuss, at the end of this section, the theoretical ideas concerning the microscopic mechanisms of flow in metallic glasses.

In many cases throughout the discussion, we will assume that the flow stress behaviour, i.e. its temperature or strain-rate dependence, is that shown by the fracture stress. This is justified, at least in the cases where fracture occurs by the pseudo-cleavage mode, since, as we have seen in the previous section, shear deformation preceeds final failure of the specimen [52]. Moreover, experience shows that the fracture stress behaviour of most crystalline metals [63, 64] and other solids is dictated by the flow stress behaviour [65-67] even when failure is brittle in character, i.e. true brittleness or the purely elastic spreading of cracks is not commonly found.

As with other dynamic processes, the temperature dependence of deformation is most important in helping to elucidate the flow mechanisms which occur at an atomic level. The stress required to produce plastic flow depends on the interatomic forces and, since these are well represented by the shear modulus, we shall compare, whenever possible, the relative temperature dependence of the flow stress (or fracture stress) with that of the shear modulus. This will provide a qualitative basis on which to decide whether plastic flow in a given metallic glass is thermally activated or not. In the latter case, the flow or fracture stress should have the same relative temperature dependence as the shear modulus.

6.1. The stress-strain behaviour

Tensile tests have been performed on several amorphous alloys. Generally, the specimens were in the form of thin strips (25 to 100 μm thick, 0.1 to 0.3 cm wide) prepared by the QR [29, 30], or the RC [31] technique or a modified version of this [40].

Fig. 22a shows a typical room temperature tensile stress elongation curve for $Pd_{80}Si_{20}$ [37]. Following an initial linear stress-strain behaviour, there is a departure from linearity and thereafter fracture occurs at the maximum stress reached. This departure from the linear behaviour occurs in a very smooth fashion. At the rather high elastic strains which obtain before failure ($\sim 2\%$) a small part of this non-linear portion of the curve must be due to non-linear elasticity. Unloading experiments as in Fig. 22b, show that irrecoverable plastic strains occur before failure

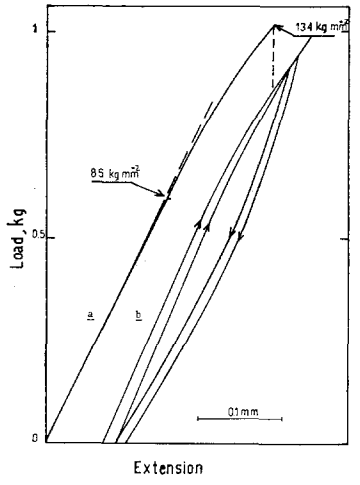

Figure 22 (a) Typical tensile stress-elongation curve for a metallic glass. $Pd_{80}Si_{20}$. (b) Unloading experiments [37].

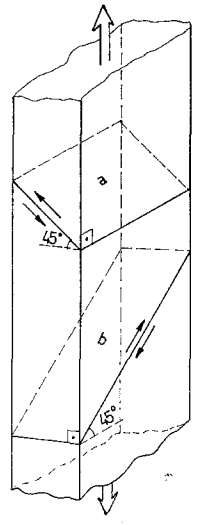

Figure 23 Schematic drawing showing at (a) the plane on which shear deformation generally occurs in metallic glass ribbons pulled in tension and at (b) another possible maximum applied shear stress plane.

and, except for a small anelastic component [69], the glass behaves in an elastoplastic fashion. At room temperature tensile plastic elongations (measured after subtracting the linear elastic part) have been reported to be between 0.1 and 0.5% [34, 37, 40] showing, as mentioned in Section 2, a macroscopically brittle behaviour.

In spite of this and of the rather high stress levels reached (as high as 2% of Young's modulus) the present author has found, in agreement with Chen and Wang's observation [69], that in general, fracture stresses are quite reproducible and not sensitive to surface conditions, handling or imperfection in grip alignment. However, in our experience, this is not the case for the elastic limit which is found to be sensitive to testing conditions.

In flat or ribbon-shaped specimens, the inhomogeneous shear deformation which eventually leads to failure occurs generally on planes whose normals form an angle of 45° to the tensile axis and the thickness vector, the shear displacement occurring normal to the width vector, see Fig. 23a. This is a plane and direction of maximum shear stress; but so is the plane whose normal forms an angle of 45° with the tensile axis and the width vector, where the shear displacement should occur along the direction normal to the thickness vector as in Fig. 23b.

However, deformation along such a plane and direction has not been observed. It is not certain whether this is due to a physical reason related to the flow behaviour or just a mechanical effect (see Addendum B).

There has been only one report of macroscopically ductile tensile behaviour [37]. This was found in $Pd_{80}Si_{20}$ when pulled at temperatures above $\sim$ 473 K. Below this temperature, the tensile elongation is 0.1% and increases rapidly above that temperature, reaching 4% at 573 K. At 525 K the stress-strain curves begin to show the occurrence of tensile instability evidenced by a maximum in the nominal tensile stress. Quite certainly, necking of the sample develops at these temperatures (no information about this is given in [37]) and fracture probably occurs along the necked zone (it is classified as a slant type fracture in [70]). As the specimens are thin strips, necking and fracture should occur along a band at an angle of 54.7° to the tensile axis, if the glass follows a Von Misses yielding criterion at these temperatures, or normal to the tensile axis, and through the thickness if it follows a Tresca criterion [71]. Both cases should be clearly distinguishable from the shear and fracture mode shown in Fig. 23a.

The small macroscopic elongations which obtain in tension, do not allow us to study plastic flow in metallic glasses in greater detail. Compression experiments are, therefore, desirable in that they overcome the problem of fast failure. Uniaxial compressive deformation in amorphous $Pd_{77.5}Cu_6Si_{16.5}$ [32, 44] $Pd_{64}Ni_{16}P_{20}$ and $Pt_{60}Ni_{15}P_{25}$ [72] have been performed recently. This was possible owing to the rather small

quenching rates required to retain the amorphous phase in these alloys, which allowed the fabrication of bulk samples suitable for compression experiments.

Fig. 24 shows the uniaxial compressive nominal stress-strain curves for $Pd_{77.5}Cu_6Si_{16.5}$ [32] at different temperatures. After a small

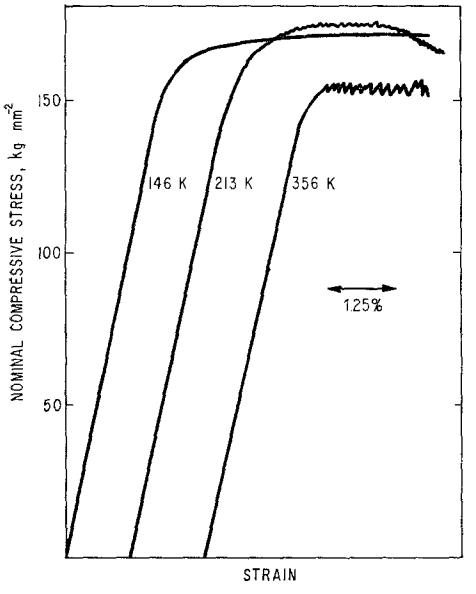

Figure 24 Uniaxial compressive nominal stress-strain curves for $Pd_{77.5}Cu_6Su_{16.5}$ at different temperatures [32].

In compression depending on temperature, the glass deforms initially in a smooth or stable way and after a certain strain continues by unstable or jerky flow and serrations [32, 72]. As the temperature is increased, the serrations become larger and the strain, during the initial stable flow, decreases until it is suppressed. This is seen in Fig. 25 which is a tracing of the recording paper of the Instrom machine.

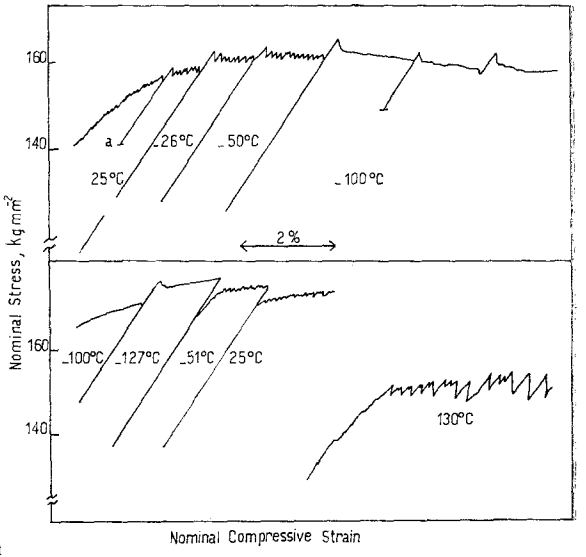

Figure 25 Tracing of the recording paper in compression experiments with $Pd_{77.5}Cu_6Si_{16.5}$.

plastic deformation (0.5 to 1%), during which one observes a positive strain hardening rate of the same order as that found in tension, the nominal stress reaches a plateau; after 1 to 2% extra strain it starts to decrease. This instability during compressive loading was considered to be due to the growth of one slip band ahead of the others causing a reduction in the load-bearing area of the sample [32]. However, some work-hardening is still apparent after correction for the loss of area due to the action of a single slip band [72]. The positive strain-hardening evidenced in these experiments could be the result of slip band intersections. This is because when an active slip band is intersected by another, the first must continue its motion by deforming into virgin material where the flow stress is larger. In addition, the stress concentration at the head of the band, which depends on the length, l, of the slip band ($\propto \sqrt{l}$) is reduced when the band is sectioned.

Serrated flow has been observed in $Pd_{77.5}Cu_6Si_{16.5}$ [32], $Pd_{64}Ni_{16}P_{20}$ and $Pt_{60}Ni_{15}P_{25}$ [72]. Serrated flow in $Pd_{77.5}Cu_6Si_{16.5}$ is suppressed below about 200 K [32]. Below this temperature deformation proceeds in a stable manner (Figs. 24 and 25). Yield drops develop when the specimen is redeformed after stopping and partially unloading (a) or not unloading (b) to change temperature.

Pampillo and Chen [32] have suggested that the unstable flow found in these experiments could be due to a partial relaxation of the atomic rearrangements produced by plastic deformation. If these rearrangements lead to a "softer glass" (e.g. destruction of compositional short range order or increase in the mean atomic volume), as discussed in Section 4, then above a certain temperature, T_0, where there is enough atomic mobility, partial relaxation of these rearrangements (e.g. regeneration of the destroyed short range order) may occur as quickly as the

rearrangements are produced: this leads to unstable flow. Below T_0 ($T_0 \approx 200$ K), the atomic mobility is too small to allow this and plastic deformation becomes stable. It is expected that the atomic mobility will be enhanced within shear bands due to the dilatance produced by plastic flow. This means that at the lower temperatures, but above T_0, a certain plastic strain may be required before unstable plastic flow sets in; this is observed in Figs. 24 and 25 and in [72] (stage I). One also expects to find yield drops when deformation proceeds after stopping for a certain time, since the relaxation of atomic rearrangements previously produced is enabled to be more complete; these yields drops should also occur below T_0. This is observed in Fig. 25.

The explanation suggested is similar to the models postulated to explain serrated flow in crystalline substitutional solid solutions [73, 74]. So far, the analogy holds qualitatively, but more experimental data are required before reaching a conclusion. It would be interesting to study the amount of stable plastic strain before unstable flow as a function of temperature and strain rate, particularly close to 200 K (− 70°C). Based on the observation that the lower stress limit σ_l of the serrations decreases with decreasing applied strain rate, Chen [72] proposed recently that the unstable flow in these glasses is due to adiabatic heating within shear bands. The heat evolved because of plastic flow is thought to be enough to raise the temperature locally to the glass transition temperature, T_g. This occurs just after a sudden yield drop and the glass then deforms by viscous flow at a stress $\sigma_l \approx \eta_{eff}\dot{\epsilon}$, where η_{eff} is the effective viscosity and $\dot{\epsilon}$ the applied strain rate; σ_l therefore decreases with decreasing $\dot{\epsilon}$ as observed. Below T_0 ($\sim$ 200 K for $Pd_{77.5}Cu_6Si_{16.5}$ [32]), the temperature increase needed to reach T_g (T_g − 200 K = 450 K for Pd–Cu–Si) becomes too large and the heat evolved by plastic flow becomes insufficient; plastic deformation becomes stable below this temperature, as observed.

Since the high temperature T_g, is considered to be reached locally, just after the yield drop, it is not clear in the model what causes the yield drop. Also the relative change in the lower stress limit, σ_l, with a change in strain rate observed ($\Delta\ln\sigma_l/\Delta\ln\dot{\epsilon} \approx 310^{-2}$) is of the order of magnitude expected for a solid with an almost athermal flow stress, but not for a substance deforming viscously for which $\Delta\ln\sigma/\Delta\ln\dot{\epsilon}$ approaches unity. Finally, as discussed in Section 4, one expects a rather small temperature rise within a deformation band specially, as emphasized by Argon [48] when deformation occurs in very narrow bands.

6.2. The temperature dependence of flow and fracture

The effect of temperature on flow and fracture of amorphous metals have been measured in $Pd_{80}Si_{20}$ [37], $Pd_{77.5}Cu_6Si_{16.5}$ [32], $Fe_{76}P_{16}C_4Si_2Al_2$, $Ni_{49}Fe_{29}P_{14}B_6Al_2$ and $Ni_{72}P_{18}B_7Al_3$ [39, 40], $Ni_{37}Fe_{37}P_{14}B_6Al_3Si_3$ [57] $Fe_{80}P_{15}C_5$ [75]. Fig. 26 shows the fracture stress and elastic limit as a function of temperature for $Pd_{80}Si_{20}$ [37] and $Fe_{80}P_{15}C_5$ [75]. The Pd–Si alloy shows a rather athermal behaviour below about 273 K: for the fracture stress σ_f the relative dependence at 200 K is $(1/\sigma_f)d\sigma_f/dT = -0.7 \times 10^{-4}$ K^{-1} and $(1/\sigma_e)d\sigma_e/dT = -5 \times 10^{-4}$ K^{-1} for the elastic limit. This last value is of the same order as that for the Young's modulus as measured with a dynamic technique [49] $(1/E)dE/dT = -2.9 \times 10^{-4}$ K^{-1}. Above 273 K, both σ_f and σ_e decrease rapidly with temperature at a rate which is much higher than that of E; -70×10^{-4} K as compared to -4×10^{-4} K (for E) at 473 K (the value for the temperature dependence of E is estimated from data for $Pd_{76}Au_{7.5}Si_{16.5}$ glass as measured with a dynamic technique [76]. The data for the Pd–Si glass shows that below about 273 K flow and fracture are probably controlled

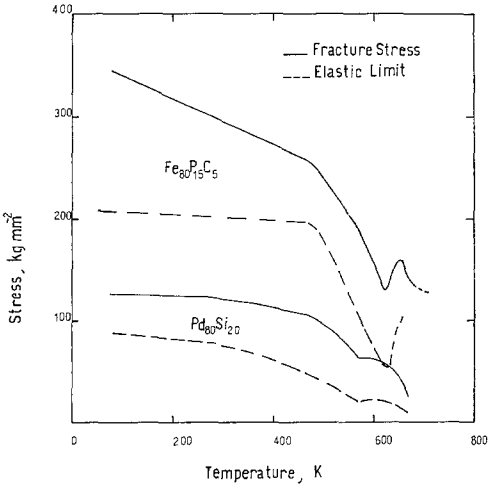

Figure 26 Fracture stress σ_f and elastic limit σ_e as a function of temperature in $Pd_{80}Si_{20}$ [37] and $Fe_{80}P_{15}C_5$ [75].

by an athermal mechanism and above that temperature by a thermally activated one. From the shape of the σ–T curves, the mechanisms acting within each temperature regime (above and below 273 K) are related in parallel since the weakest one prevails at each temperature.

A similar change in mechanisms is manifested by a change in the strain rate sensitivity of the fracture stress, as shown in Fig. 27. This change is consistent also with two parallel processes which, in all probability, are the same acting above and below 273 K (Fig. 26). The fracture stress σ_f follows the same trend as the elastic limit σ_e at the higher temperature. The behaviour at the lower temperature, however, is rather unexpected, since a strain rate insensitive flow behaviour is difficult to reconcile with a fracture stress which decreases with strain rate. The fracture mode is reported to change from a "slant type" at the high temperature/slow strain rate regime, to a "square type" in the low temperature/high strain rate regime [70].

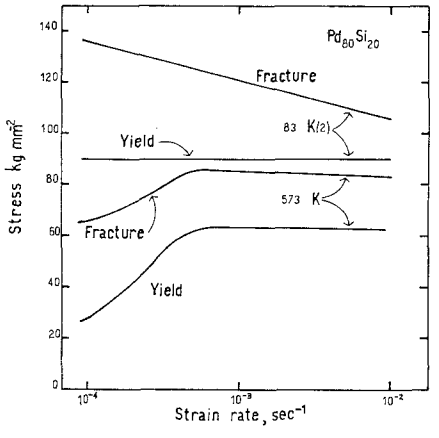

Figure 27 Fracture stress σ_f and elastic limit σ_e in $Pd_{80}Si_{20}$ as a function of elongation rate [70].

A similar comparison between the tensile data of $Fe_{80}P_{15}C_5$ and the shear modulus, as measured in a dynamic way for a glass of similar composition [40] shows for the elastic limit σ_e a behaviour which is very similar to that of $Pd_{80}Si_{20}$; the temperature at which a change in the flow mechanism is evidenced appearing at 473 K. The fracture stress σ_f on the other hand, shows a strong temperature dependence below 473 K, but still the mechanisms acting below and above 473 K are related in parallel. It is rather difficult to understand the fact that plastic flow (elastic limit) is insensitive to temperature within a certain temperature region, while fracture shows a strong temperature dependence. A plausible explanation for this behaviour is that although flow is athermal, fracture in the $Fe_{80}P_{15}C_5$ glass is controlled by an environmental effect which becomes gradually suppressed as the temperature is lowered. We are inclined to believe, however, that the reason for this behaviour may lie in the sensitivity of the elastic limit to testing conditions, as already mentioned in Section 6.1, and the difficulty encountered in making an accurate measurement of σ_e with a stress-strain curve such as that shown in Fig. 22a. However, the possible existence of an environmental effect could only be ruled out by experiment, e.g. deformation within an inert atmosphere. At higher temperatures, 573 and 623 K for the $Pd_{80}Si_{20}$ and $Fe_{80}P_{15}C_5$ glasses respectively, σ_e and σ_f increase with increasing temperature, leading to a maximum in the σ–T curve. This seems to be due to a partial crystallization of the glasses at the testing temperatures [37].

Fig. 28 shows the 0.2% compressive flow stress in $Pd_{77.5}Cu_6Si_{16.5}$ bulk glass as a function of temperature [32]. We compare the flow stress temperature behaviour with that of the Young's modulus, as measured with a dynamic technique

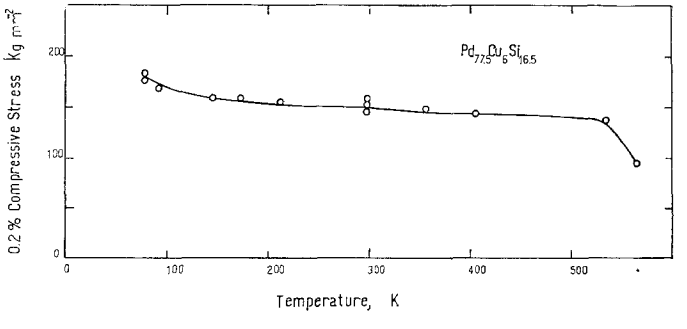

Figure 28 The 0.2% compressive flow stress in $Pd_{77.5}Cu_6Si_{16.5}$ bulk glass as a function of temperature [32].

(we compare with the modulus of $Pd_{81}Si_{19}$ [77] which is expected to have about the same temperature dependence as that for the Pd–Cu–Si glass). It is found [40] that the flow stress depends on temperature roughly as E above 250 K and below this temperature the flow stress increases with decreasing temperature at a relative rate which is greater than that for the modulus. This indicates the existence of a thermally activated mechanism. At about 500 K the compressive flow stress decreases rapidly with increasing temperature in a way similar to that found in the $Pd_{80}Si_{20}$ and $Fe_{80}P_{15}C_5$ glasses at 273 and 473 K respectively.

The temperature dependence of the fracture stress of $Ni_{72}P_{18}B_7Al_3$, $Ni_{49}Fe_{29}P_{14}B_6Al_2$, $Fe_{76}P_{16}C_4Si_2Al_2$ [40] and $Fe_{37}Ni_{37}P_{14}B_6Al_3Si_3$ [57] was investigated by Pampillo and Polk. Fig. 29 shows the fracture stress as a function of temperature. One finds two kinds of behaviour: for the $Ni_{72}P_{18}B_7Al_3$ and $Ni_{49}Fe_{29}P_{14}B_6Al_2$ the fracture stress increases monotonically with decreasing temperature. The $Fe_{76}P_{16}C_4Si_2Al_2$ and $Ni_{37}Fe_{37}P_{14}B_6Al_3Si_3$, on the other hand, display an embrittling effect at 100 and 175 K, respectively. This effect is discussed in Section 6.3.

Fig. 30 [40] shows a plot of the ratio between the shear stress at fracture τ and the shear modulus (measured by dynamic techniques [40, 77], for glassy $Ni_{72}P_{18}B_7Al_3$, $Ni_{49}Fe_{29}P_{14}B_6Al_2$, $Fe_{76}P_{16}C_4Si_2Al_2$ and $Pd_{77.5}Cu_6Si_{16.5}$; in the last case for the 0.2% compressive flow stress [33]. Firstly, we note here the rather high values found for this ratio, which mean that the elastic strains at fracture are of the order of 2%. Secondly, keeping in mind the considerations made in the second paragraph of Section 6, the plot suggests that for each glass, above a certain temperature, T_0 the shear flow stress depends on temperature as the shear modulus, and below that temperature plastic flow is controlled by a thermally activated mechanism.

Accepting that two different mechanisms are controlling plastic flow above and below T_0, we can see that the two are related in series since at each temperature the hardest is in control. One also may separate the contributions of each

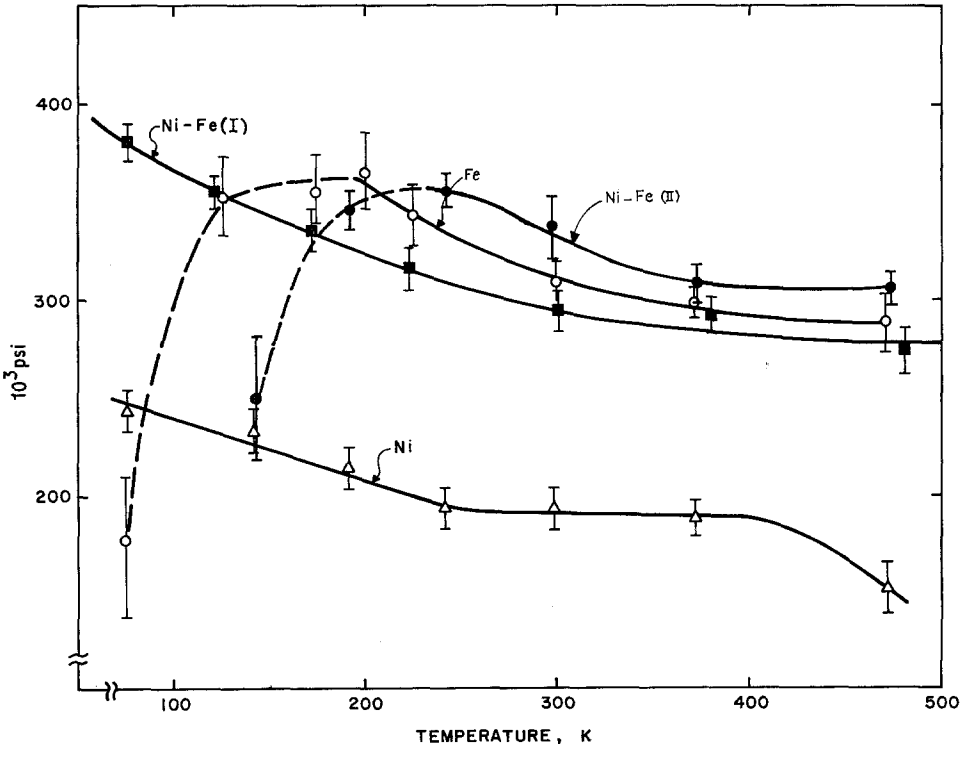

Figure 29 Fracture stress of $Ni_{72}P_{18}B_7Al_3$ (Ni), $Ni_{49}Fe_{29}P_{14}B_6Al_2$ [Ni–Fe (I)], $Fe_{76}P_{16}C_4Si_2Al_2$ (Fe) [40] and $Fe_{37}Ni_{37}P_{14}B_6Al_3Si_3$ [Ni–Fe (II)] [57], as a function of temperature.

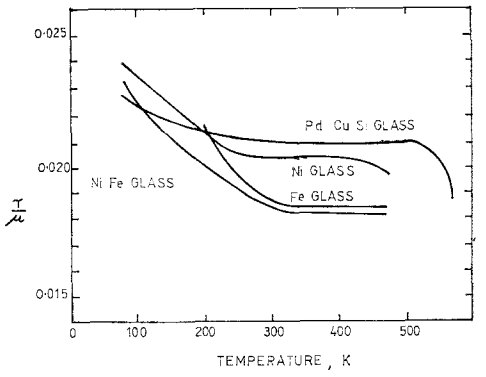

Figure 30 The ratio τ/μ between the shear stress at fracture and the shear modulus for $Fe_{76}P_{16}C_4Si_2Al_2$, $Ni_{49}Fe_{29}P_{14}B_6Al_2$ and $Ni_{72}P_{18}B_7Al_3$ and for the shear flow stress (from the 0.2% compressive flow stress) for $Pd_{77.5}Cu_6Si_{16.5}$ glasses [40].

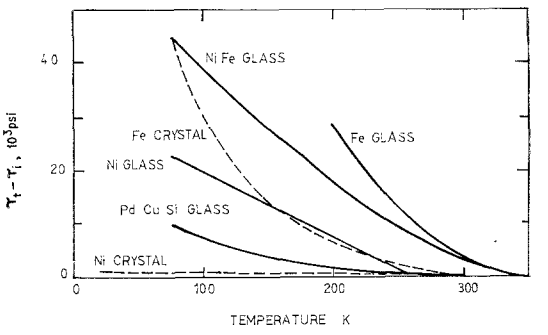

Figure 31 Temperature dependent part of the shear stress at fracture or shear flow stress of the glasses in Fig. 29. Also included is the effective shear stress τ^* in pure F [78] and Ni [79] single crystals [40].

mechanism to the flow stress. The part contributed by the thermally activated mechanism, obtained by subtracting the athermal stress level from the total flow stress, is shown in Fig. 31 [40], together with the equivalent data for Fe [78] and Ni [79] single crystals (as a matter of comparison, the athermal shear stress level which is 100 kg mm^{-2} in the Fe-base glass is 1 kg mm^{-2} in Fe single crystals). The possibility of separating the flow stress into two stress components, one athermal (τ_i) and the other thermally activated, is a standard practice in the discussion of plastic flow in crystalline metals and has been well substantiated by experimental data [79-82]. The possibility of conducting the same separation in the metallic glasses is, admittedly, somewhat speculative at this time and needs more experimental proof. However, it allows a comparison with the crystalline metals. As we shall see, this comparison points to some interesting factors that deserve further investigation.

Pampillo and Polk [40] have pointed out that the character of the bonding in a metal, or more specifically, whether the bond energy has a strong angular dependence as in Fe and other bcc metals, as opposed to the central forces in Ni and other fcc metals, is probably not lost when the crystal lattice is distorted to obtain the structure of the glass. Possibly, this is the only memory of its parent crystal left within the glass. They further argued that since it is this "covalent" character which provides the important factor leading to the strong temperature dependence of the stress in Fe and other bcc metals [83] (high Peierls-Nabarro stress) the same factor may be playing a similar role in the metallic glasses. Furthermore, the magnitude of the temperature effect on the flow stress in the different glasses, giving the range of behaviours shown in Fig. 31 would be due to a "dilution" or "enhancement" of the covalent character of the atomic bonding, by other elements within the glass. This would be similar to the case of solution softening of bcc metals such as Fe. It has been suggested that the reduction of the thermal component of the flow stress in Fe by Ni additions, is due to a filling of the d levels of Fe [84]. One would expect this to decrease the angular dependence of the bond energy and, therefore, the Peierls-Nabarro stress.

A directional bonding between the metallic atoms and the metalloids in the glass may also be expected. Elements such as C, Si, P in Fe may reinforce the covalent character of the bonding. On the other hand, this character would be somewhat diluted in the Ni-base and the Pd–Cu–Si glass where the only directional bonding may come from the metal–metalloid interactions. The extent of "compositional short-range order" in each glass, may also play an important role here.

The above discussion implicitly assumes that plastic flow in metallic glasses occurs by the motion of dislocations. This point will be discussed in Section 7.

6.3. A ductile-brittle transition in Fe-based glasses

The embrittling effects of temperature on $Fe_{76}P_{16}C_4Si_2Al_2$ [40] and $Ni_{37}Fe_{37}P_{14}B_6Al_3Si_3$ [57] is manifested by a catastrophic decrease of the fracture stress with decreasing temperature at

100 and 175 K respectively. The microscopic fracture modes found in these two glasses are different to those in glasses showing no embrittling effects. As discussed in Section 5.2, the latter fail by the pseudo-cleavage microscopic mode at all temperatures tested while the former only fail by that mode at temperatures somewhat above room temperature. Below room temperature failure occurs normal to the tensile axis; the fracture topography found is shown in Figs. 14 and 15 and has been discussed in Section 5.2.

The fact that the "brittle transition" is concomitant with a change in the microscopic fracture mode seems to rule out an environmental effect as a possible cause of brittleness. From this fact, it is apparent that the brittleness phenomenon is similar to the ductile cleavage transition in crystalline Fe and mild steel. An important factor related to this transition in crystalline Fe is the temperature dependence of the friction stress [68], i.e. the stress required to move dislocations within the crystal. As seen in Section 6.2, the temperature dependence of the flow stress in the glasses containing Fe appears to be even greater than that in Fe crystals. However, the $Ni_{49}Fe_{29}P_{14}B_6Al_2$ glass also shows a strong temperature dependence but no brittle transition. Probably, brittleness in this glass occurs at temperatures below the lowest temperatures reached in the tensile experiments, i.e. 77 K. An observation which indicates that this may be so, is shown in Fig. 32. Indentation with a microhardness machine at liquid nitrogen temperature, 77 K, is found to produce cracking; no cracking is found under similar conditions at room temperature. The much higher strain rates produced under the indenter, compared with that in a tensile test, may very well shift the transition to temperatures above 77 K.

The absence of an embrittling effect in the $Fe_{80}P_{15}C_5$ glass, Fig. 26, is worth noting here and certainly deserves further experimental investigation. An effect which, as mentioned in Section 5.2, is related to brittleness, is that of fragmentation. No mention is made in [75] of such an effect in the $Fe_{80}P_{15}C_5$ glass.

6.4. The hydrostatic pressure dependence of the flow stress in a metallic glass

Davis and Kavesh [55], have deformed a $Pd_{77.5}Cu_6Si_{16.5}$ glass in tension and uniaxial compression under high hydrostatic pressure (6.9 kbar $\approx 10^5$ psi). Fig. 33a shows the compressive stress-strain curve for a specimen deformed in an interrupted way, i.e. first at 1 atm and then at high pressure. In this way the flow stress at the two pressures and the same strain can be compared without resorting to different specimens.

The flow stress level increases with hydrostatic pressures by about 0.5 $kbar^{-1}$. Unstable flow (stress serrations) seems to be unaffected by the superimposed high pressure. Fig. 33b shows the tensile stress-strain curve at 1 atm and 6.9 kbar. Both the elastic limit and the fracture stress are increased by hydrostatic pressure. Surface examination of the specimens after deformation shows that the highly inhomogeneous mode of deformation is unaffected by pressure.

The relative pressure dependence measured is

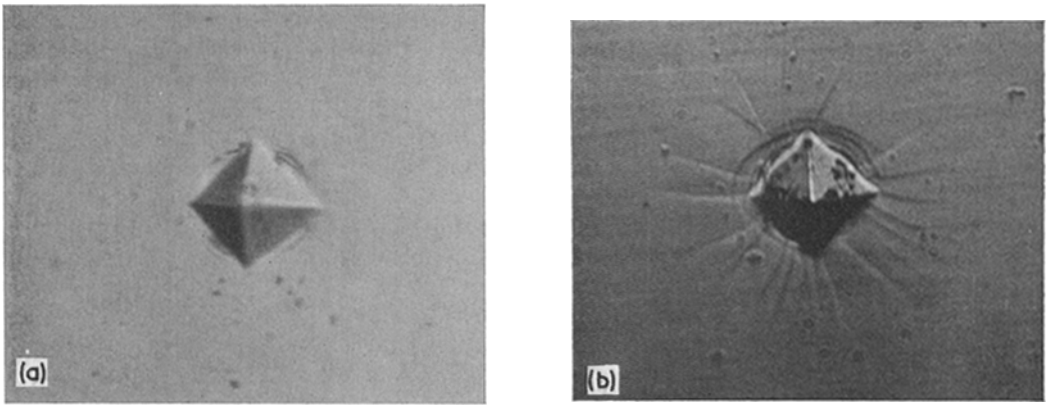

Figure 32 Microhardness indentation on $Ni_{49}Fe_{29}P_{14}B_6Al_2$ glass (a) at room temperature and (b) at liquid nitrogen temperature.

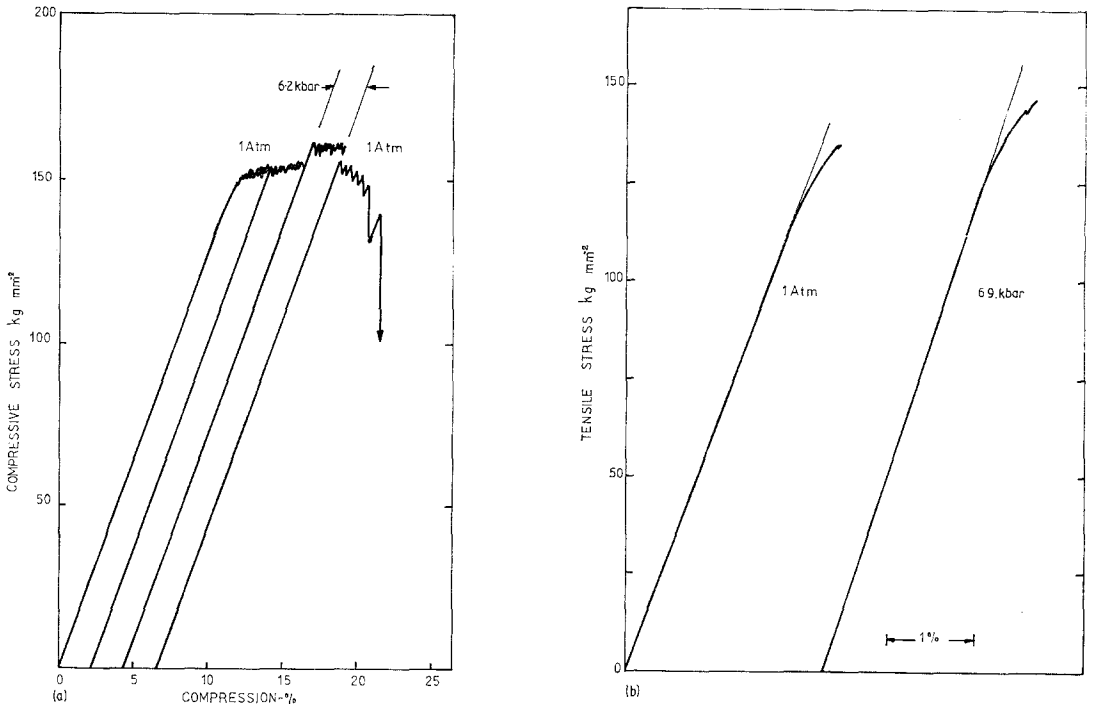

Figure 33 (a) Compressive stress strain curve for $Pd_{77.5}Cu_6Si_{16.5}$ glass deformed at 1 atm and 6.9 kbar [55]. (b) Tensile stress-strain curves for the same glass at 1 atm and at 6.9 kbar [55].

$\Delta \ln\sigma/\Delta P = (5 \pm 0.7)\ 10^{-6}$ bar^{-1}. As pointed out by Davis *et al.*, this is the same dependence found in crystalline metals such as Fe, Ni, Cu and Al. For these metals, the relative pressure dependence is equal to that of the moduli, i.e. $\Delta \ln\sigma/\Delta P = \Delta \ln\mu/\Delta P = \Delta \ln B/\Delta P$, where B is the bulk modulus [85].

The tensile fracture surface topography obtained on specimens that failed at high pressure was discussed at the end of Section 5.1.

6.5. Creep

Creep measurements in a metallic glass were first reported by Chen and Turnbull for $Au_{77}Ge_{13.6}Si_{9.4}$ [12]. The experiments demonstrated for the first time the existence of a rheological solid glass/metastable liquid transition. Creep measurements were conducted within the temperature range 286 to 297 K, i.e. just below the glass transition temperature, $T_g = 297$ K. Within the above temperature range, the amorphous alloy behaves as a viscous liquid with a stress independent viscosity $\eta = \sigma/3\dot{\epsilon}$, where $\dot{\epsilon}$ is the tensile creep rate, ranging from 10^9 to 10^{12} P (the stress range was 0.03 to 1.4 kg mm^{-2} and the creep rates $\dot{\epsilon} \approx 10^{-4}$ to 10^{-5} sec^{-1}).

The temperature dependence of viscosity does not follow an Arrhenius relationship (the apparent activation energy ranges from 62 to 114 kcal gat^{-1}) but rather a Fulcher-Vogel relation: $\eta = \eta_0 \exp(A/T - T_0)$. This η–T relation was found to be independent of how the temperature was reached. If the temperature is suddenly changed, the viscosity is found to lag behind the temperature change. Chen and Turnbull [12] take this to be evidence that the viscosity depends primarily on configuration rather than on temperature. However, from their data, we find that by the time a temperature change of 2 K has been completed, the viscosity has changed by a factor of 1.4 to 1.8. A simple calculation shows that this is equivalent to the contribution of a thermally activated mechanism with an activation enthalpy of 30 to 45 kcal mol^{-1}. The experiments rule out the possibility of creep due to a Nabarro-Herring mechanism acting in a microcrystalline structure. One expects such structure to change irreversibly with temperature [12].

Chen and Goldstein [87] made similar measurements on $Pd_{79.5}Au_4Si_{16.5}$, $Pd_{79.5}Ag_4Si_{16.5}$ and $Pd_{77.5}Cu_6Si_{16.5}$ near their glass transition temperatures, 645, 640 and 646 K, respectively.

At low stress and below the temperature T_a, at which $\eta = 10^{12}$ P, the creep behaviours of the alloys were similar to that of $Au_{77}Ge_{13.6}Si_{9.4}$ already described. However, above T_a creep became non-Newtonian and the viscosity was, therefore, stress-dependent. Annealing the samples at $T > T_a$ had no effects on the creep behaviour near T_a and hence phase seperation was disregarded as the possible cause of the anomalous behaviour. It is possible, however, that incipient crystallization took place during creep at $T > T_a$ but did not occur on annealing the samples under zero stress. This possibility is prompted by the experiments in a Pd–Si glass reviewed next.

Maddin and Matsumoto [70] carried out extensive creep measurements on $Pd_{80}Si_{20}$ in the temperature range 373 to 473 K ($T_g = 655$ K). From this investigation, an important finding is the effect of an applied tensile stress on crystallization. Fig. 34 shows the temperature-time-transformation diagram for $Pd_{80}Si_{20}$. As can be seen, a stress of 48 kg mm^{-2} can shorten the crystallization time at, for instance 540 K, by a factor of 18. Creep experiments were conducted at temperatures and during times within the region where the solid remained amorphous.

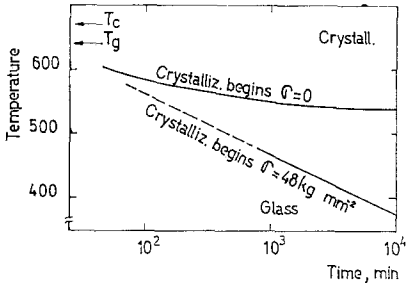

Figure 34 Temperature-time-transformation diagram for $Pd_{80}Si_{20}$, showing the effect of an applied stress on crystallization [70].

Analysis of the steady-state creep yielded a $\dot{\epsilon} \propto \sigma^{1.6}$, a strain rate–stress relation: hence creep was non-Newtonian. One is faced with the fact that crystalline alloys show such high strain-rate sensitivities and become "superplastics" when their grain sizes are very small (generally micron size). One is tempted to interpret the results of Maddin and Masumoto as showing the existence of a microcrystalline structure. However, as is well known, superplastics owe their stable grain size to a duplex structure. Amorphous metals have a single phase and, as already emphasized by Chen and Turnbull [12], one expects a microcrystalline structure to behave irreversibly with respect to temperature.

The steady-state creep rates followed an Arrhenius temperature relation, yielding a stress-dependent activation enthalpy $H(\tau)$, which we have plotted from Maddin and Masumoto's data in Fig. 35. The decreasing enthalpy with increasing applied shear stress is consistent with a stress-aided thermally activated process. The value extrapolated to zero stress is about 0.56 eV. Maddin and Masumoto point out the closeness of the activation enthalpy to that for the viscosity of liquid Ni (0.52 eV). The possibility also exists that creep is controlled by the diffusion of only one of the atomic species in the glass if the diffusivities of the different species are very different. In particular, Si has been pointed out as a fast diffusing element in Pd–Si glasses [32]; therefore, one would expect a low activation energy. It is clear that diffusion measurements in metallic glasses would be highly desirable in order to be able to draw more conclusions from the creep experiments.

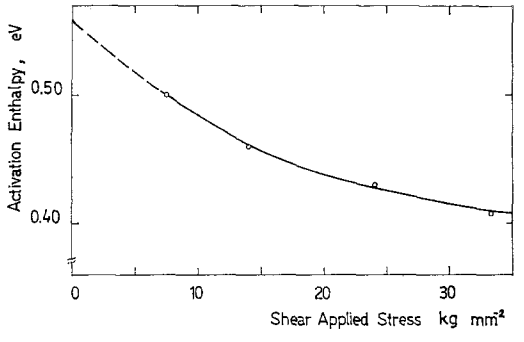

Figure 35 Activation enthalpy for steady state creep in $Pd_{80}Si_{20}$ as a function of the applied shear stress (data from [70]).

The shear stress activation volumes, v, which result from the stress-dependent activation enthalpy (Fig. 35) $v = \partial H^{+}/\partial\tau$, where τ is the applied shear stress, decrease from 130 Å^3, at the lower stresses to 50 Å^3 at the higher ones (Maddin and Masumoto [70] give a value which is smaller than this, 25 Å^3, because they erroneously calculate the activation volume as the change in activation enthalpy with tensile stress). The above values are about 10 and 4 atomic volumes respectively. Maddin and Masumoto [70] consider that the steady-state creep is due

to the motion of atoms across distances of about one atomic spacing. However, the values for the shear stress activation volumes show that a co-operative motion of atoms is involved in the thermally activated event. The transient creep is considered to occur by the transfer of atoms from the random close packed arrangement to a more "regular crystalline" array which grows with time and, once formed, ceases to contribute to the creep rate because it becomes harder than the matrix. Steady-state creep must result when these regions or zones stop growing. The reason for this cessation of growth (although the zones should be more stable than the glass) is not specified. This model, prompted by the finding that applied stresses promote crystallization, could be further tested by dynamic measurements of the elastic moduli as a function of deformation under creep conditions. This may enable the harder "more regular" zones to be detected.

Finally, we should mention that the creep process studied by Maddin and Masumoto corresponds to the regime of rapidly decreasing flow (fracture) stress with increasing temperature (Fig. 26). A similar fast decrease in the flow stress as a function of temperature occurs in $Pd_{77.5}Cu_6Si_{16.5}$ (Fig. 28), in $Fe_{80}P_{15}C_5$ (Fig. 26), and in $Ni_{72}P_{18}B_7Al_3$ (Fig. 29).

7. Theoretical ideas about flow mechanisms in amorphous metals

The experimental observations reviewed so far conclusively demonstrate the existence of plastic flow in metallic glasses, i.e. the irrecoverable distortion of the solid by means other than the creation of free surfaces. At temperatures well below the glass transition temperature, plastic flow occurs by inhomogeneous shear deformation, as indicated by the markings which appear on the free surface of a deformed metallic glass specimen; the solid chooses this mode of deformation rather than homogeneous deformation because the latter would probably require a higher stress.

This has been demonstrated recently by Li [89] for an amorphous solid which is thought to be formed by the introduction of a network of closely spaced dislocations into a crystal, i.e. the dislocation network provides the required distortions which produce an amorphous structure out of a crystal. Inhomogeneous shear (rigid displacement of two surfaces, Fig. 36b) occurs at a critical shear stress which is about half that required for homogeneous shear deformation (Fig. 36a). Moreover, the amorphous structure constructed in this way would still deform at a much lower stress, about 1/20 that for homogeneous deformation, by the motion of a dislocation through the "dislocation lattice" (Fig. 36b). The experimental proof that this is so is given by the fact that shear slip bands which terminate within the solid have been observed [32, 55]. This fact has also been pointed out for amorphous polymers [51, 90].

Up to this point, the dislocation may only be considered as a Volterra dislocation, i.e. the boundary between slip and unslipped portions of the solid. We believe that as such, the linear defect responsible for plastic flow in amorphous metals at low temperatures has been established. The important question remaining is whether this macro or Volterra dislocation is made up of discrete dislocations whose strength is of the order of atomic size. If so, their motion controls the velocity of the shear band and hence the macroscopic plastic properties, through their own dynamic behaviour. We would like to point out here that the flow stress temperature data on Ni, Ni–Fe and Fe-based glasses reported by Polk and Pampillo [39, 40], gives support to this idea: it is quite difficult to believe that a slip band considered as a macro-dislocation could move by stress-aided thermally activated motion.

Gilman [90] proposed that, at low enough temperatures, where the viscous relaxation time becomes much longer than the time for plastic flow, adjacent shear events will be correlated and hence flow may be described by the motion of dislocations of atomic size strength. Gilman estimates that for viscosities higher than $\sim 10^{11}$ P, flow should occur by the motion of dislocation lines. At lower viscosities, i.e. at higher temperatures, shear events should become uncorrelated and flow becomes viscous, as in liquids or crystals, at very high temperatures, where diffusion becomes the controlling factor.

For a dislocation in an amorphous solid it is not possible to define a Burgers vector. It is only possible to define a displacement vector $\boldsymbol{\delta}$, or closure failure, accumulated along a circuit around the linear defect, by its elastic strain field, i.e. $\boldsymbol{\delta} = \oint(\partial \mathbf{u}/\partial l)\mathrm{d}l$ ($\mathbf{u}$ is the elastic displacement field of the dislocation and $\mathrm{d}l$ an element of the circuit around it). Contrary to dislocations in crystals, this displacement vector will fluctuate along the defect line because the displacement of each atom along the dislocation line, towards its

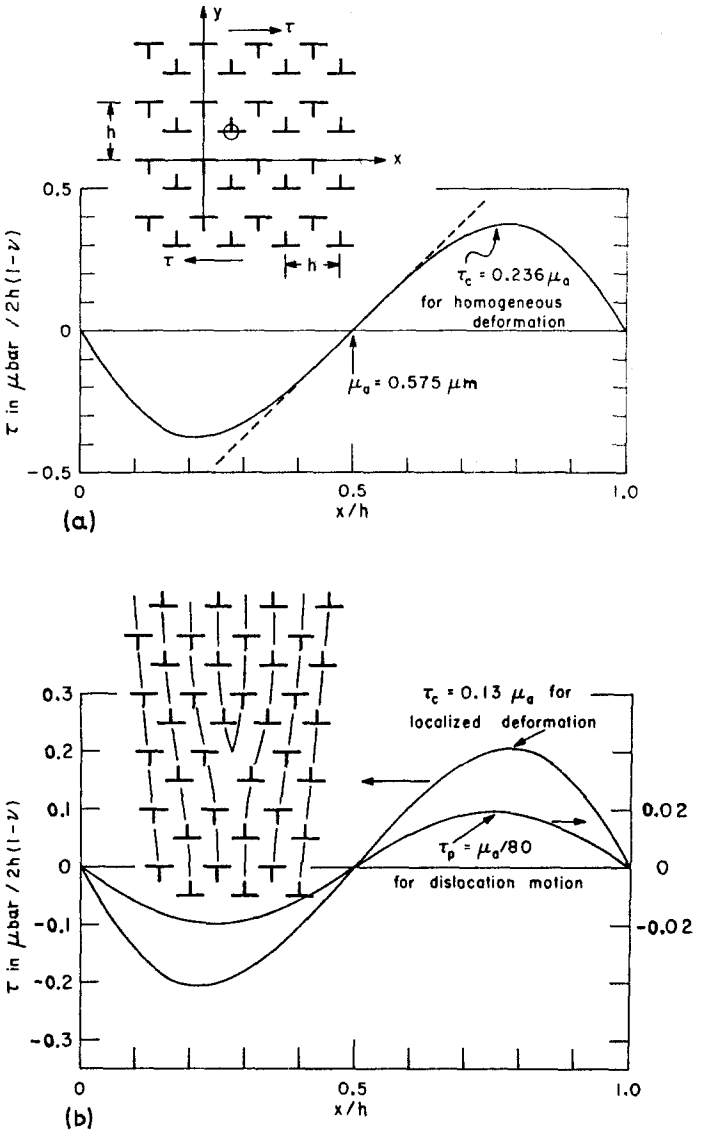

Figure 36 Dislocation lattice model for an amorphous metal. (a) Homogeneous shear deformation. (b) Localized deformation and dislocation moving through the dislocation lattice [79].

new equilibrium position, will vary in magnitude and direction [90].

Ashby and Logan [91] have brought up the question of whether such a dislocation in an amorphous solid is stable; it is possible to think that the elastic strain field of the dislocation could be relaxed by displacements of the atoms; this is possible in the glass (but not in the crystal) because the atomic positions are not fixed and unique [91]. Likewise, we may consider that the dislocation core will become enlarged owing to small atomic relaxations around its centre. This will decrease the mobility of the dislocation, just as blunting of the tip of a crack makes its motion more difficult. As the chance to relax, for atoms around the core, depends on the dislocation velocity, the effect leads to a rapid damping of the dislocation for velocities $v < d/\tau$ where d is the core size and τ the atomic relaxation time. This atomic relaxation time will be smaller than that for atoms far from the dislocation due to the dilatance associated with the core of the dislocation. Dislocations in amorphous solids should be considered then as dynamic defects introduced at stress concentrations (just as is the case of a focuson or a crowdion introduced into a crystal by an atomic collision).

Gilman [90] has suggested that the most

important factor controlling the dynamics of dislocation motion in amorphous solids comes from the dilation created by the severe shear distortion at the core of a dislocation. This dilation decreases the effective viscosity η_c at the core of the dislocation relative to that of the matrix. For a narrow dislocation, about an atomic distance wide, Gilman estimates $\eta_c = \eta_0(1 + 1.4B/\alpha T)^{-1}$, where B is a constant of the order of unity and α is the volume thermal expansion. Unfortunately, the meaning of the viscosity of the matrix, η, at temperatures far below the glass transition temperature becomes unclear and hence the above equation does not allow one to predict plastic properties such as temperature dependence of the flow stress or its magnitude. It does show that the atomic mobility within the core of a dislocation in an amorphous solid will be much higher than that outside it, rendering the dislocation mobility. However, as noted above, this enhanced atomic mobility will probably promote the growth of the dislocation core and decrease its mobility.

The magnitude of the shear stress required to produce plastic flow by dislocation motion in an amorphous solid was first considered by Argon [92]. The amorphous solid is thought to be formed by introducing into a crystal a series of randomly oriented tetragonal distortions that create the glassy structure. The stress required to move a dislocation that existed in the original crystal is estimated from the theory of solution-hardening by tetragonal distortions; the distortional strain used to evaluate this stress is estimated from the width of the first peak of the Radial Distribution Function (RDF) of the particular glass considered. For amorphous Ag–Au and $Ni_{80}P_{20}$, Argon obtains $\tau_0 = 0.003\mu$ and 0.01μ. These values are lower than but of the same order as those shown in Fig. 30. Li [89] has considered the distortions which create the amorphous structure as arising from a "dislocation lattice" (Fig. 36). By assuming the distance h between dislocations in the lattice to be about two nearest neighbours distance, Li calculates the stress required to move a "Volterra dislocation" through the dislocation lattice, obtaining $\tau_0 = 0.0125\mu$ which is close to the values shown in Fig. 30. The distance between dislocation in the dislocation lattice could also be estimated by using the radial distribution function of the glass, in a way similar to the estimation made by Argon for the tetragonal distortions [92]. However, for the purpose of estimating the critical flow stress, the value used ($h = 2b$) is probably quite realistic.

Pampillo and Chen [32] have pointed out that the existence of a compositional short range order in metallic glasses must contribute to the critical flow stress. This is because a dislocation that moves through such a solid must destroy part of the short range order. The energy to create such a disorder is provided by the external applied stress and, at low enough temperatures, cannot be introduced with the aid of thermal fluctuations. This mechanism would give an athermal flow stress. For a disordering surface of say $\gamma = 300$ erg cm^{-2}, the drag stress due to short range compositional ordering is about $\tau = \gamma/b \approx 0.02\mu$. At higher temperatures, where there is some atomic mobility, a dislocation may move through the compositional short range order aided by diffusion (probably due to the fastest diffusing atomic species [93]). The flow stress should then decrease with increasing temperature. The two mechanisms, i.e. the athermal destruction of compositional short range order and that aided by diffusion, are related in parallel. Such a decrease in the flow stress, marking a change between parallel mechanisms, is observed in $Pd_{80}Si_{20}$, $Fe_{80}P_{15}C_5$ (Fig. 26); $Pd_{77.5}Cu_{16.5}Si_6$ (Fig. 28), and $Ni_{72}P_{18}B_7Al_3$ (Fig. 29).

Maddin and Masumoto [70] have also shown that in $Pd_{80}Si_{20}$, at relatively high temperatures, flow produces incipient crystallization (see Fig. 34). This will induce a driving force aiding plastic flow, and the flow stress would decrease with increasing temperatures. This mechanism could also explain the decrease in flow stress at higher temperatures. The temperature region where this occurs in each glass will be related to its relative stability.

As already discussed, if flow is due to dislocation motion, there will be a temperature above which atomic mobility becomes large and shear events become uncorrelated. This puts a limit on possible diffusion-controlled dislocation motion mechanisms. Electron microscopic studies by replica techniques of surface slip markings, as a function of temperature, could give important information about the transition from one type of flow to the other.

A different point of view on the mechanism of plastic flow in metallic glasses is that of Leamy *et al.* [34], who suggest that plastic flow propagation (and concentration of plastic flow) is due to adiabatic heating caused by the dissipation

of plastic work. This heating is assumed to be enough to soften the glass when the temperature within the bands approaches the glass transition temperature T_g. The model is similar to that proposed to explain plastic flow in amorphous polymers well below their glass transition temperature [94, 95].*

We have already discussed this topic in connection with the inhomogeneous plastic flow in metallic glasses (Section 4), and concluded that the temperature rise within slip bands should be small. However, under certain geometrical conditions, adiabatic heating effects could occur. For instance, if deformation or fracture conditions are such that portions of a sample become isolated (because the rest of the sample has already failed), the heat extraction becomes difficult, the solid heats up locally, elongates more uniformly because of the ensuing softening, leading to even worse heat extraction conditions. Eventually, T_g is reached and viscous flow develops rapidly. We believe this is the case shown in Fig. 4 and for the veins or triple vein intersections (Fig. 9b).

Another model that makes use of the glass–liquid transition to explain plastic flow in amorphous metals is that of Spaepen and Turnbull [53]. In this case, the glass–liquid transition is stress induced, i.e. the free volume needed to reach the transition is induced by the hydrostatic tension at stress concentrations. Regions which dilate in such a manner become fluid and propagate following the maximum shear stress plane. The mechanism is considered to be self sustaining since the fluid band carries, at its head, the hydrostatic tension needed to dilate the glass. A fluid layer develops across the whole sample and viscous flow between two solid planes occurs until failure of the fluid layer. The vein pattern found on fracture surfaces is considered to be evidence of the high fluidity within the slip band (see Section 5.1). However, it is not understood why the band remains fluid once across the whole specimen. The stress normal to the band, at this stage, is even lower than the tensile stress.

Davis and Kavesh [55] have measured the pressure dependence of the tensile and compressive flow stress, σ, in a glassy metal (see Section 6.4). They concluded that since the relative pressure dependence found for σ is of the order of that expected for the bulk modulus B, the data could be in agreement with the model of Spaepen and Turnbull or that of Gilman [90]. In this last model, the free volume is considered to be formed at the core of dislocations. The pressure dependence measured could also be in agreement with models which do not make use of free volume. In the model of Spaepen and Turnbull, one expects the stress σ_d required to reach a certain critical dilation, to have the same relative pressure dependence as the bulk modulus B [55]. One should consider also that the flow stress σ must be higher than σ_d. The extra stress, σ_v, is the stress required to maintain a shear strain rate $\dot{\gamma}$ at an effective viscosity η_{eff} within the shear band. To a first approximation, $\sigma_v = \eta_{eff}\dot{\gamma}$ and the relative pressure dependence of σ is $\Delta \ln\sigma/\Delta P = (\sigma_d/\sigma)\Delta \ln B/\Delta P + (\sigma_v/\sigma)\Delta \ln \eta_{eff}/\Delta P$. As $\dot{\gamma}$ within the fluid band may reach values of the order of 10^{-1} to 1 sec^{-1} ($\dot{\gamma} \approx \dot{l}/h$, where $\dot{l}$ is the compression rate, $\sim 10^{-4}$ cm sec^{-1}, and h the slip band thickness, ~ 1 to 10 μm), σ_v may reach high values (probably as high as 1/20 or 1/10 of σ; at these stresses the strain-rate/stress relation is, however, no longer linear). If the effective viscosity η_{eff}, is sensitive to pressure, this should lead to a significant contribution to the relative pressure dependence. One expects a strong pressure dependence of viscosity for a fluid which is close to its glass–liquid transition.

The model of Spaepen and Turnbull is similar to those proposed to explain plastic flow below the glass transition temperature in amorphous polymers [97-99]. These models have been criticized for not being able to explain flow under pure shear conditions [100]. However, one may consider that shear flow is accompanied by dilation, as occurs in granular materials, and that this shifts the atomic arrangements towards those prevailing near T_g. This has been proposed for amorphous polymers [101] but seems to be in contradiction with experimental data [102].

Finally, whether or not discrete dislocations of strength, approximating to atomic size are responsible for plastic flow in amorphous metals, will have to be decided by experiment. Almost certainly, these experiments will have to be of an indirect nature, because direct observation with the electron microscope is improbable. The normal diffraction contrast mechanism, which reveals strain fields in crystalline metals, is absent in amorphous solids. Moreover, as emphasized before, dislocations in these solids may be dynamic defects which only exist for short periods and only during their motion. In

*It has been proved experimentally that in polymers plastic flow does occur under isothermal conditions [96].

this case, other possible techniques such as decoration (probably via preferential crystallization on dislocations) or etch pits, may be inoperative. In all probability, the information will have to come from macroscopic plastic flow behaviour. The flow (fracture) stress-temperature behaviour found for amorphous metals [32, 37, 39, 40, 57, 70, 75] is a first step in this direction.

8. Summary

Several papers have appeared in the last few years dealing with the plastic flow and fracture properties of metallic glasses. The main findings of these experimental investigations are:

(1) Metallic glasses are ductile on a microscopic scale. Macroscopically they behave in a brittle manner;

(2) Plastic flow is concentrated in sharp shear bands. There are observations which seem to show that there is a change in the atomic structure within the slip bands;

(3) Contrary to crystalline metal behaviour, plastic deformation in some metallic glasses can be reversed by flow along the same shear bands which produced an initial permanent set;

(4) The inhomogeneous deformation is responsible for the lack of macroscopic ductility;

(5) For some glasses (based on Pd or Ni), at all temperatures, fracture occurs on planes previously defined by a slip band. Final failure involves an opening displacement normal to this plane, and leaves a typical "vein pattern". Cracking is nucleated at several places on the fracture plane at what appears to be hard impurity particles or small crystallized portions of the glass;

(6) Other glasses (based on Fe) show a more brittle behaviour. Fracture occurs normal to the tensile axis and does not follow planes defined by prior shear deformation. The microtopographical fracture features resemble, in cases, those on high strength alloys (dimpled rupture);

(7) Temperature plays an important role in the brittleness of these last glasses. There is an apparent ductile-brittle transition at some temperature below room temperature;

(8) The fracture stress of metallic glasses based on Fe or Ni–Fe is strongly temperature dependent. The form of this dependence is similar to that found for the flow or fracture stress of crystalline metals. For some glasses (based on Fe or Ni–Fe) this dependence is even stronger than that of bcc crystalline metals;

(9) At a temperature approaching the glass transition temperature and under small stress, deformation occurs by Newtonian viscous flow;

(10) In $Pd_{80}Si_{20}$ at temperatures below T_g, crystallization can be stress aided.

Several theoretical ideas have been advanced to explain flow in metallic glasses:

(1) It has been proposed that at temperatures well below T_g, plastic deformation in amorphous metals occurs via dislocation motion. The motion of a Volterra dislocation through a "dislocation lattice"-induced random structure, has been shown to be easier than homogeneous shear or rigid plane displacement;

(2) The question has been raised whether dislocations in amorphous solids can be stable. It has also been proposed that these linear defects in glassy metals are dynamic defects;

(3) Another proposition is that flow and its concentration into shear bands occurs as a consequence of adiabatic heating due to plastic work, which causes a drastic reduction of the effective viscosity;

(4) A third proposition is that the hydrostatic stress at stress concentrations induces enough free volume to render portions of the solid fluid, which then flow viscously;

(5) Fracture has been considered to be the result of the high temperature reached within shear bands due to adiabatic heating;

(6) Similarly, fracture is considered to occur by the breaking up of a fluid layer (the slip band) induced by tensile stresses leaving the typical "vein pattern";

(7) Finally, it has been proposed that fracture is a result of "pseudo-cleavage" crack propagation on a plane defined (by weakening) by the prior shear deformation. The veins found on fracture surfaces are the result of collisions between "pseudo-cleavage" cracks;

(8) It has been pointed out that the strong temperature dependence of the fracture stress indicates a stress-induced thermally activated mechanism, probably via the motion of atomic size strength dislocations;

(9) It has been suggested that the similarity of the stress-temperature characteristics to those of crystalline metals is related to the character of the atomic bonding.

9. Glassy metals as technological materials

So far it has been shown that glassy metals are strong, reaching fracture stresses as high as

270 kg mm^{-2} (380 $\times$ 10^3 psi). Improvements in melting practice, in producing the liquid from which the glasses are formed, and in the quenching rates obtained, will probably produce even higher strengths by preventing the formation of second phase particles. However, even at these very high strengths these solids are not as brittle as oxide glasses and can accommodate bending stress by plastic flow.

Metallic glasses are now produced at high speeds (1800 m min^{-1}) into shapes such as ribbon, tape or wires [4]. Tapes as wide as 1.3 cm have been made. Their thickness is generally limited, because of the high quenching rates required, to about 0.013 cm and wire diameters range between 0.013 and 0.04 cm [4].

Some of the glasses obtained so far contain rather inexpensive alloying elements. Moreover, the production technique avoids a semi-fabricated stage and, therefore, must also reduce the production cost.

One may expect, therefore, that glassy metals will be produced as low-cost high-strength materials that will find applications as fibre-reinforcing elements in plastics or in rubber e.g. tyre cords. Another possible structural application [103] is in inertial energy storage devices, i.e. flywheels. In this case they could be used with advantage as bare filaments if their good strength properties still hold for fairly long lengths of filament. This has not yet been demonstrated. The high hardness and good corrosion properties of these solids will also make them useful in applications related to cutlery [4, 103, 104]. Many other applications envisaged for these solids would make use of their other physical properties e.g. magnetic (magnetic bubbles), and elastic (acoustic lines) properties [4, 104]. These are, however, beyond the scope of this review.

Acknowledgements

Thanks are due to D. E. Polk, J. J. Gilman, J. C. M. Li and L. A. Davis for many fruitful discussions on the subject. Thanks are also due to L. A. Davis and J. W. Cahn for their patience in reviewing the manuscript.

Addendum in proof

A. Fracture toughness and fatigue growth measurements

Davis [A1] recently reported on measurements of fracture toughness and fatigue crack growth at room temperature in glassy alloys. Fracture toughness measurements (K_C) were conducted in $Ni_{48}Fe_{29}P_{14}B_6Al_3$ glass, using a tensile single-edge notch specimen. The notch was introduced by prefatiguing specimens of uniform cross-section. For $Ni_{39}Fe_{38}P_{14}Al_3$ and $Ni_{49}Fe_{29}P_{14}B_6Si_2$ glasses, tests were conducted on centre-cracked specimens prepared by introducing a $\sim$ 0.1 mm hole in the centre of each specimen by electric discharge machining. Cracks were grown from the hole by fatigue before final fracture.

Fatigue crack growth measurements were made in the $Ni_{39}Fe_{38}P_{14}B_6Al_3$ glass by following the crack tip with a microscope at a magnification of $\times$ 105. Table I gives the results and other geometrical and mechanical data:

TABLE I

Alloy glass	Ni_{48}	Ni_{39}	Ni_{49}
K_C (kg mm$^{-3/2}$)	120	62	30
Yield stress (kg mm^{-2})	190	214	240
Thickness (μm)	25	43	72
Width (mm)	0.4	1.7	0.76
Crack growth rate, da/dn (mm/cycle)	$2 \times 10^{-8}\Delta K^{2.25}$		

The width, thickness and yield stress of the specimens are such that plane strain conditions are probably met only for the Ni_{49} glass. The increase in toughness K_C obtained for Ni_{49}, Ni_{39} and Ni_{48}, in that order, is thus considered to be due to a change from plane strain to approaching plane stress conditions. The K_C value obtained for the Ni_{49} glass is probably a valid plane-stress toughness value, i.e. K_{IC}, except for the fact that the specimens were allowed to fail during cyclic loading, i.e. the maximum stress intensity factor used during fatigue was about equal to the fracture toughness measured. This may somewhat increase the toughness measured due to an effect of the notch root radius [A2].

The value obtained (30 kg mm$^{-3/2}$) is comparable to the toughness expected at the same yield strength level for quenched and tempered steels prepared by conventional melting practice [A3]. Improved melting practice such as vacuum induction melting or vacuum arc remelting has shown substantial improvements in fracture toughness of steels [A3]. This should also hold for metallic glasses where, as we have seen in Sections 5.1 and 5.2, second-phase impurity particles seem to play an important role as crack nuclei.

When plane strain conditions prevailed, fracture surfaces were found to be parallel to the

tensile axis and microscopic topography was similar to that found in $Fe_{76}P_{16}C_4Al_3B_1$ and $Ni_{37}Fe_{37}P_{14}B_6Al_3Si_3$ below room temperature (Figs. 14b and 15) i.e. when pseudo-cleavage was suppressed. Since the glasses tested for toughness also show the pseudo-cleavage mode of fracture when tested as unnotched strips, plane stress conditions seem to inhibit this mode in a way similar to lowering the test temperature.

The fatigue crack propagation rate measured in the Ni_{39} glass is slightly higher than that of crystalline ferrous alloys when compared at equal cycle stress intensity ΔK. However, when the data are compared at equal $\Delta K/E$, where E is the Young's modulus, the glassy metal behaves similarly to crystalline ferrous alloys.

Scanning electron microscope observations of fatigue striation markings on the fracture surfaces of the Ni_{39} glass show that the spacing between striations is six times larger than da/dn. Davis suggests that this is because the oscillations in local direction, which produce the striations, occur with a period of the order of the plastic zone size.

B. Orientation of shear plane

Davis [A4] has shown that if the sides of the ribbons are polished down such that the width-to-thickness, w/t, ratio is < 8, fracture occurs along a plane at $\sim 53°$ to the tensile axis and parallel to the thickness vector. This is the correct shear band plane for unstable yielding in flat ribbons which follow a Von Mises yield criterion and are pulled in uniaxial tension (one must allow a correction for the elastic strain before yielding). In the loaded state the angle is 54.7°. Davis argues that in the wider specimens ($w/t > 8$) fracture occurs by antiplane strain crack propagation before general yielding is reached. The crack front is supposed to move in the width direction on a plane at 45° to the tensile axis and the crack opening displacement is normal to the width vector. The question of why the wider specimens do not fail following the Von Mises criterion is not answered, however.

Although Davis' suggestion that the wider strips ($w/t > 8$) do not reach general yielding may be valid in some cases, we have often observed that portions of a fractured specimen show surface slip band markings which run straight across and parallel to the width vector. These are shear bands which run across the specimen and have not reached fracture. They show that general yielding on planes at 45° to the tensile axis and to the thickness vector does occur. We believe the reason for having through-the-thickness shear in the wider strips is simply that the state of stress is not perfectly uniaxial tension but rather plane stress with a small but non-zero stress along the width. This is because the specimens are not perfectly rectangular in cross-section. Their thickness decreases slightly towards the edges. Under this state of stress, yielding will occur on planes at 45° to the tensile axis and the thickness vector.

References

1. B. B. BAGLEY and D. T. TURNBULL, *J. Appl. Phys.* **39** (1968) 5681.
2. S. MADER, *J. Vacuum Sci. Tech.* **2** (1965) 35.
3. W. KLEMENT, IV., R. H. WILLENS and P. DUWEY, *Nature* **187** (1960) 869.
4. A. L. ROBINSON, Research News; Glassy Metals: No longer a laboratory curiosity. *Science*, **182** (1973) 908.
5. *Scientific American*, **230** (3) (1974).
6. P. DUWEZ, *Trans. ASM* **60** (1967) 606.
7. B. C. GIESSEN and C. N. J. WAGNER, in "Liquid Metals", edited by S. Beer (Marcel Decker, New York, 1974).
8. R. H. WILLENS and B. C. GIESSEN, in "The use of Phase Diagrams in Ceramic, Glass and Metal Technology", edited by A. M. Alper (Academic Press, New York, 1970).
9. B. G. BAGLEY, H. S. CHEN and D. TURNBULL, *Mat. Res. Bull.* **3** (1968) 159.
10. N. VALENKOV and E. W. POROJ-KOSIC, *Z. Krist.* **75** (1936) 196.
11. J. D. BERNAL, *Nature* **185** (1960) 68.
12. H. S. CHEN and D. TURNBULL, *Acta Met.* **11** (1969) 104.
13. *Idem, J. Chem. Phys.* **48** (1968) 2560.
14. *Idem, J. Appl. Phys. Lett.* **10** (1967) 284.
15. C. V. GOKULARATHNAM, *J. Mater. Sci.* **9** (1974) 673.
16. T. R. ANANTHARAMAN and C. SURYANARAYANA, *ibid* **6** (1971) 1111.
17. D. TURNBULL, Strasbourg Conference on Disordered Systems (September, 1973).
18. D. E. POLK, *Acta. Met.* **20** (1972) 485.
19. *Idem*, private communication.
20. R. RAY, B. C. GIESSEN and N. J. GRANT, *Scripta Met.* **2** (1968) 357.
21. D. E. POLK, C. H. BENNETT and D. TURNBULL, *Acta Met.* **19** (1971) 1295.
22. R. RAY, W. GIESSEN and N. GRANT, *Scripta Met.* **2** (1968) 357.
23. A. S. NOWICH and S. MADER, *I.B.M. J. Res. and Dev.* **9**, 358.
24. G. S. CARGILL, III, *J. Appl. Phys.* **41** (1970) 12; **41** (1970) 2248.

25. R. C. CREWDSON, Ph.D. Thesis, California Institute of Technology, Pasadena, California (1966).
26. G. S. CARGILL, *J. Appl. Phys.* **41** (1970) 1.
27. H. S. CHEN and B. K. PARK, *Acta Met.* **21** (1973) 395.
28. M. COHEN and D. TURNBULL, *J. Chem. Phys.* **31** (1959) 1164; **34** (1961) 120.
29. H. S. CHEN and C. E. MILLER, *Rev. Sci. Instrum.* **41** (1970) 1237.
30. E. BABIC, E. GIRT, R. KRSNIK, B. LEONTIC and I. ZORIC, Proceedings of the International Conference on Metastable Metallic Alloys, Brela, Yugoslavia, (1970); *Fizika*, suppl. to **2**.
31. E. POND JUN and R. MADDIN, *Trans. Met. Soc. AIME* **245** (1969) 2475.
32. C. A. PAMPILLO and H. S. CHEN, *Mat. Sci. Eng.* **13** (1974) 181.
33. H. J. LEAMY, private communication.
34. H. J. LEAMY, H. S. CHEN and T. T. WANG, *Met. Trans.* **3** (1972) 699.
35. D. E. POLK, unpublished work (1972).
36. H. S. CHEN, H. J. LEAMY and M. J. O'BRIEN, *Scripta Met.* **7** (1973) 415.
37. T. MASUMOTO and R. MADDIN, *Acta Met.* **19** (1971) 725.
38. D. E. POLK and C. A. PAMPILLO, unpublished work.
39. *Idem, Scripta Met.* **7** (1973) 1161.
40. C. A. PAMPILLO and D. E. POLK, *Acta Met.* **22** (1974) 741.
41. R. RAY, private communication (1973).
42. C. A. PAMPILLO, unpublished work.
43. D. E. POLK and D. TURNBULL, *Acta Met.* **20** (1972) 493.
44. C. A. PAMPILLO, *Scripta Met.* **6** (1972) 915.
45. J. J. GILMAN, *J. Appl. Phys.* **44** (1973) 675.
46. K. H. ROSCOE, in "Structure, Solid Mechanics and Engineering Design", edited by M. Te'eni (Wiley-Interscience, New York, 1971).
47. K. H. ROSCOE, *J. Strain Analysis* **3** (1968) 57.
48. A. S. ARGON, in "Inhomogeneous Plastic Deformation", edited by R. E. Reed-Hill (ASM, Metals Park, Ohio, in press).
49. B. S. BERRY and W. C. PRICHET, *J. Appl. Phys.* **44** (1973) 3122.
50. Z. S. BASINSKI, *Proc. Roy. Soc. London* **A240** (1957) 229.
51. J. C. M. LI, C. A. PAMPILLO and L. A. DAVIS, in "Deformation and Fracture of High Polymers", edited by H. H. Kausch, J. A. Hassell and R. I. Jaffe (Plenum, New York, 1974).
52. C. A. PAMPILLO and A. C. REIMSCHUESSEL, *J. Mater. Sci.* **9** (1974) 718.
53. F. SPAEPEN and D. TURNBULL, *Scripta Met.* **8** (1974) 563.
54. D. G. SAFFMAN and G. I. TAYLOR, *Proc. Roy. Soc. London* **A245** (1958) 312.
55. L. A. DAVIS and S. KAVESH, *J. Mater. Sci.* **10** (1975) 453.
56. G. LUETJERING and L. A. DAVIS, unpublished work.
57. C. A. PAMPILLO and D. E. POLK, unpublished work (1973).
58. J. R. LOW, JUN, *Eng. Fracture Mech.* **1** (1968) 47.
59. C. D. BEACHEM, in "Fracture", edited by H. Liebowitz (Academic Press, New York, 1968).
60. A. R. C. WESTWOOD, in "Fracture of Solids", edited by J. J. Gilman and D. C. Drucker (Interscience, New York, 1962).
61. A. S. ARGON, *Proc. Roy. Soc. London* **A250** (1959) 482.
62. L. A. DAVIS, unpublished work.
63. J. R. LOW, JUN, in "Fracture", edited by B. L. Averbach *et al.* (Wiley, New York, 1959) p. 68.
64. A. H. COTTRELL and A. KELLY, *Endeavour* **25** (1966) 27.
65. D. M. MARSH, in "Fracture in Solids", edited by D. C. Drucker and J. J. Gilman (Wiley, New York, 1963) p. 143.
66. D. M. MARSH, *Proc. Roy. Soc. London* **A282** (1964) 33.
67. J. D. MEAKIN and N. J. PETCH, in "Fracture of Solids", edited by D. C. Drucker and J. J. Gilman, (Wiley, New York, 1963) p. 393.
68. N. J. PETCH, in "Fracture", Vol. I, edited by H. Liebowitz (Academic Press, New York, 1968) Ch. 5.
69. H. S. CHEN and T. T. WANG, *J. Appl. Phys.* **41** (1970) 5338.
70. R. MADDIN and T. MASUMOTO, *Mat. Sci. Eng.* **9** (1972) 153.
71. R. HILL, "Mathematical Theory of Plasticity" (Oxford, 1950).
72. H. S. CHEN, *Scripta Met.* **7** (1973) 931.
73. A. PORTEVIN and F. LE CHATELIER, *Compt. Rend. Acad. Sci., Paris* **176** (1923) 507.
74. A. H. COTTRELL, *Phil. Mag.* **44** (1953) 829.
75. T. MASUMOTO, Seminar on "Metallic Materials", Sendai, Japan (1973).
76. H. S. CHEN, H. J. LEAMY and M. BARMATZ, *J. Non-Crystalline Solids* **5** (1971) 444.
77. M. BARMATZ, to be published.
78. T. NAKADA and A. KE, *Acta Met.* **16** (1968) 903.
79. H. CONRAD, in "The Relation between the Structure and Mechanical Properties of Metals" (H.M.S.O., London, 1963).
80. H. CONRAD, *Mat. Sci. Eng.* **6** (1970) 265.
81. H. CONRAD, *Phil. Mag.* **5** (1960) 745.
82. J. C. M. LI, *Canad. J. Phys.* **45** (1967) 493.
83. J. FRIEDEL, "Dislocations" (Addison-Wesley, New York, 1964).
84. R. J. ARSENAULT, *Acta Met.* **15** (1967) 501.
85. P. HAASEN and A. W. LAWSON, *J. Metallkde* **49** (1958) 280.
86. C. HERRING, *J. Appl. Phys.* **21** (1950) 437.
87. H. S. CHEN and M. GOLDSTEIN, *ibid* **43** (1972) 1642.
88. M. F. CULPIN, *Proc. Roy. Soc. London* **B70** (1957) 1069.

89. J. C. M. LI, in "Distinguished Lectures in Materials Science" (Marcel-Dekker, to be published).
90. J. J. GILMAN, *J. Appl. Phys.* **44** (1973) 675.
91. M. F. ASHBY and J. LOGAN, *Scripta Met.* 7 (1973) 513.
92. A. S. ARGON, to be published.
93. C. A. PAMPILLO and A. E. VIDOZ, *Acta Met.* **14** (1966) 313.
94. F. H. MULLER and K. JÄCKEL, *Kolloid Z.* **129** (1952) 145.
95. I. MARSHALL and A. B. THOMSON, *Proc. Roy. Soc. A* **221** (1954) 541.
96. P. I. VICENT, *Polymer* **1** (1960) 7.
97. M. LITT, D. J. KOCH and A. V. TOBOLSKY, *J. Macromol. Sc* . **B1** (1967) 433, 587.
98. J. D. FERRY and R. STRATTON, *Kolloid Z.* **171** (1960) 107.
99. S. NEWMAN and S. STRELLA, *J. Appl. Polymer Sci.* **9** (1965) 2297.
100. R. E. ROBERTSON, *J. Chem. Phys.* **44** (1966) 3950.
101. A. W. CHRISTIANSEN, E. BAER and S. V. RADCLIFFE, *Phil. Mag.* **24** (1971) 451.
102. C. S. PAMPILLO and L. A. DAVIS, *J. Appl. Phys.* **42** (1971) 4674.
103. Materials Research Report. Materials Research Center, Allied Chemical, October 1973.
104. Chemical and Engineering News, November 1973, p. 248.
A1. L. A. DAVIS, *J. Mater. Sci.*, in press.
A2. J. F. KNOTT, "Fundamentals of Fracture Mechanics" (Butterworths, London 1973) p. 137.
A3. W. S. PELLINI, NRL Report 6957 (1969).
A4. L. A. DAVIS, *Scripta Met.*, in press.

Received 1 December and accepted 9 December 1975.